Earthq Eng & Eng Vib (2008) 7:345-368 **DOI**: 10.1007/s11803-008-1001-x

Design of bridges against large tectonic deformation

I. Anastasopoulos†, G. Gazetas‡ , V. Drosos§, T. Georgarakos* and R. Kourkoulis*

National Technical University, Athens, Greece

Abstract: The engineering community has devoted much effort to understanding the response of soil-structure systems to seismic ground motions, but little attention to the effects of an outcropping fault offset. The 1999 earthquakes of Turkey and Taiwan, offering a variety of case histories of structural damage due to faulting, have (re)fueled the interest on the subject. This paper presents a methodology for design of bridges against tectonic deformation. The problem is decoupled in two analysis steps: the first (at the *local* level) deals with the response of a single pier and its foundation to fault rupture propagating through the soil, and the superstructure is modeled in a simplified manner; and the second (at the *global* level) investigates detailed models of the superstructure subjected to the support (differential) displacements of Step 1. A parametric study investigates typical models of viaduct and overpass bridges, founded on piles or caissons. *Fixed–head* piled foundations are shown to be rather vulnerable to faulting–induced deformation. End–bearing piles in particular are unable to survive bedrock offsets exceeding 10 cm. Floating piles perform better, and if combined with *hinged* pile–to–cap connections, they could survive much larger offsets. Soil resilience is beneficial in reducing pile distress. Caisson foundations are almost invariably successful. Statically–indeterminate superstructures are quite vulnerable, while statically–determinate are insensitive (allowing differential displacements and rotations without suffering any distress). For large–span cantilever–construction bridges, where a statically determinate system is hardly an option, inserting resilient seismic isolation bearings is advantageous as long as ample seating can prevent the deck from falling off the supports. An actual application of the developed method is presented for a major bridge, demonstrating the feasibility of design against tectonic deformation.

Keywords: fault rupture; earthquake; soil-structure interaction; bridge; viaduct; pile group; caisson foundation; finite elements

1 Introduction — bridges on top of fault: recent evidence

In many large magnitude earthquakes, the causative fault ruptures all the way to the surface ("outcrops"). Structures on top of the resulting surface fault scarp may undergo significant differential movements that could lead to failure — often catastrophic. Seismic codes have thus prohibited construction in the *"immediate vicinity"* of seismically active faults. But for long facilities and structures such as water channels, tunnels, pipelines, embankments, and long bridges crossing several geologic formations, such a prohibition has often been impossible to respect. Moreover, past and recent earthquakes have revealed that survival of structures *"on top of a fault"* is not impossible — even when fault displacements are large (on the order of *meters*).

In fact, the three 1999 earthquakes in Turkey (Kocaeli and Düzce-Bolu) and Taiwan (Chi-Chi), provided many examples of satisfactory structural performance (Youd *et al*., 2000; Erdik 2001; Bray 2001; Ulusay *et al*., 2002), serving as an actual confirmation of the older belief that structures can be designed against large tectonic displacements (Duncan and Lefebvre, 1973; Niccum *et al*., 1976; Youd 1989; Berrill 1983).

Nevertheless, several bridges were damaged due to surface faulting in the 1999 Chi-Chi earthquake (Kawashima, 2001; Pamuk *et al*., 2005). Two such examples are illustrated in Fig. 1. The first (Fig. 1(a)) shows a prestressed concrete bridge, the Bei-Fung Viaduct in Fung-Yan City (photos adapted from Hwang, 2000). The Chelungpu thrust fault crossed its south abutment with an upthrust of about 7 m. The result: collapse of two spans of the bridge due to differential displacement between the piers. The second example is the 17-span prestressed concrete Wu-Shi Bridge, subjected to about 2 m of upthrust at a 40° angle to its longitudinal axis. As shown in Fig. 1(b), two decks collapsed and most of its piers were severely damaged (mostly shear failures). Interestingly, one of its caisson foundations survived the direct "hit" by the outcropping fault, sustaining shear failure (Kawashima, 2001). The

Correspondence to: George Gazetas, National Technical University, Heroon Polytechneiou 9, 15780, Zografou, Athens, Greece
Tel: +30210 772 4075; Fax: +30210 772 2405
E-mail: gazetas@ath.forthnet.gr
†Adjunct Lecturer; ‡Professor; §Post-doctoral Researcher; *PhD Candidate

Supported by: OSE (the Greek Railway Organization) Under the Grant No. 107/2004
Received August 9, 2008; **Accepted** October 23, 2008

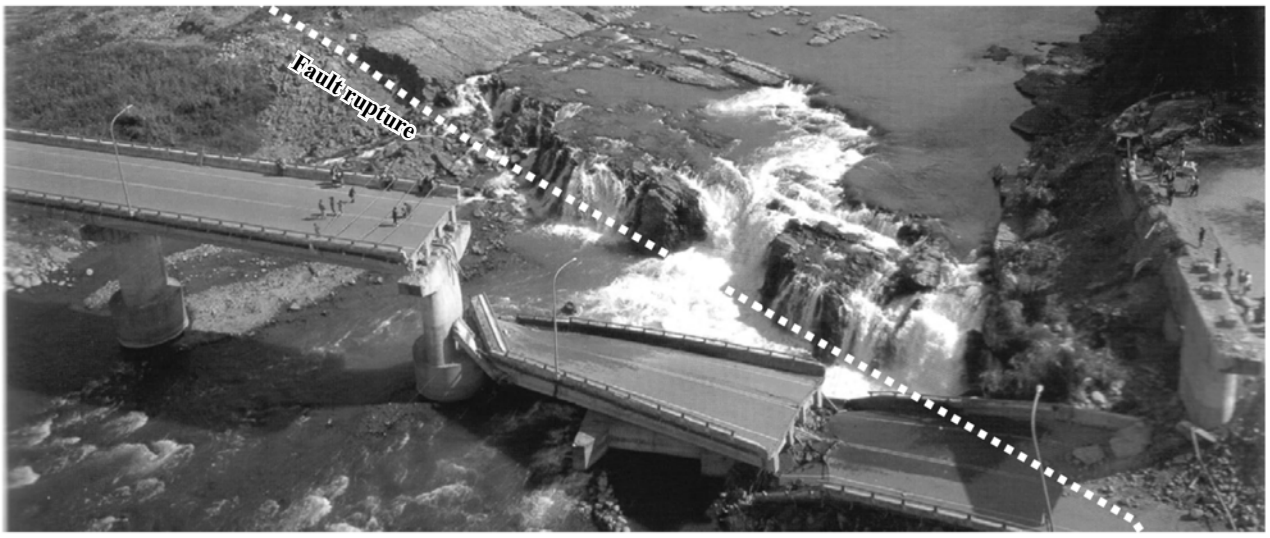

(a) Collapse of two spans of the Bei-Fung Bridge

(b) Collapse of two spans and pier shear failure of the Wu-Shi Bridge

Fig. 1 Examples of bridge failures due to tectonic dislocation in the 1999 Chi-Chi (Taiwan) earthquake. Both bridges were subjected to upthrust of the order of 5 m due to surface rupturing of the Chelungpu thrust fault. (photos adapted from Hwang, 2000)

performance of the Shi-Wei Bridge (Pamuk *et al*., 2005) was similar.

Bridge failures, but also successes, were reported after the 1999 Turkey earthquakes (Ulusay *et al*., 2002; Pamuk *et al*., 2005). One such case is the failure of the 100 m Arifiye Overpass, near Adapazari. Consisting of four simply supported pre-stressed concrete spans, it was crossed by the 2 m offsetting fault; all spans fell off due to unseating.

Figure 2 illustrates another example: the Kaynasli Viaduct of the Trans-European Motorway. During the Düzce-Bolu earthquake, this seismically-isolated 2.3 km long viaduct was crossed by the North Anatolian fault and subjected to a strike-slip offset on the order of 1.5 m. The decks were supported through pot bearings with a capacity for multi-directional sliding. Special energy dissipating units, viscous dampers, and stoppers were installed (Kawashima, 2001). The mostly 49 m high piers were founded on pile-groups consisting of 12 piles 1.8 m in diameter. As shown in Fig. 2(a), the faulting-induced deformation was responsible for the development of substantial horizontal displacements and rotations of the piers (Figs. 2(b) and 2(c)). As a result, the deck was subjected to about 1.2 m of differential displacement (Fig. 2(d)), barely avoiding collapse due to the restraint provided by the stoppers (Fig. 2(e)). However, although the piles crossed by the fault were damaged, the integrity of the pile–cap system was not sacrificed.

Evidently, such failures are the result of a seismic design which did not systematically study the consequences of fault imposed deformations. To bridge the apparent gap in our understanding, recent research efforts combining field studies, centrifuge model testing, and numerical modeling (Anastasopoulos and Gazetas, 2007a, b; Bransby *et al*., 2008; Faccioli *et al*., 2008; Anastasopoulos *et al.,* 2007, 2008) have culminated in the development of a validated methodology for analysis and design of foundation–structure systems against surface fault rupture. It was shown that *foundation continuity and stiffness* are critical for the survival of buildings.

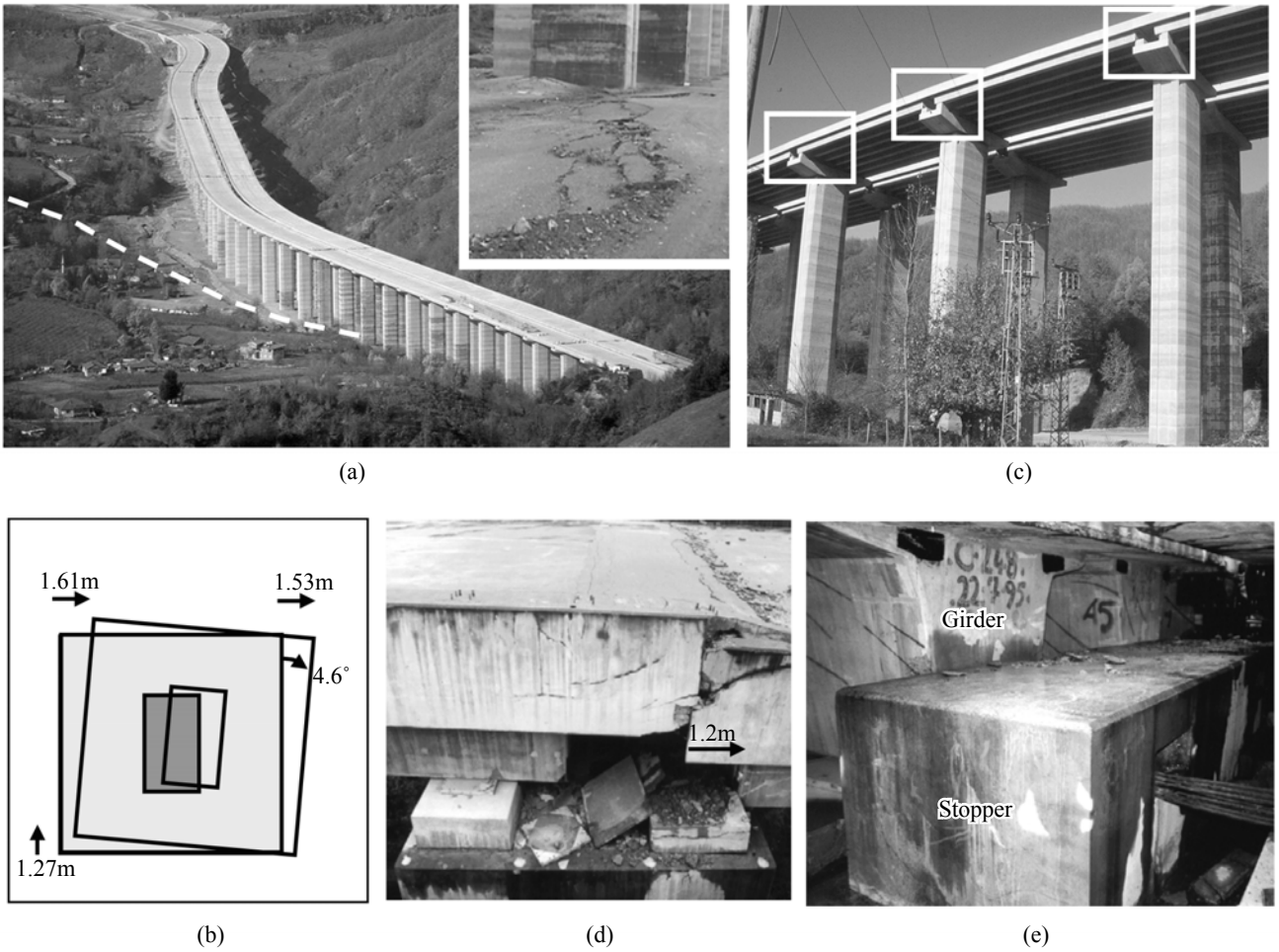

Fig. 2 Failure of the Bolu Viaduct in the 1999 Düzce (Turkey) earthquake. The strike-slip surface rupture of the North Anatolian fault crossed the bridge (a), generating displacements and rotations of the piers (b). As a result, the isolated bridge deck was subjected to about 1.2 m of differential displacement (c, d). Deck collapse was avoided only due to restrain provided by massive concrete stoppers (e)

However, for bridges, such continuity is meaningless since bridges are founded on separate supports. While a building on a continuous and stiff foundation may "convert" the imposed dislocation to rigid-body rotation without being substantially distressed, a bridge cannot avoid the differential displacement between its supports (piers). As attested by the previously discussed case histories, such differential displacement may cause structural failure or deck fall, depending on the type of the superstructure.

The basic goal of this paper is to develop a fundamental methodology for bridge design against large tectonic deformation. Since this work was part of a research project in Greece, emphasis is placed on normal faulting (the dominant mode in Greece).

2 Problem definition and analysis methodology

The problem investigated herein and the employed analysis methodology is illustrated schematically in Fig. 3. The analysis of the bridge–foundation system subjected to faulting–induced deformation is conducted in two steps, in which the interaction between rupture, soil, foundation, and superstructure is rationally taken into account. Specifically:

In Step 1 (*local* level), the response of a single bridge pier subjected to fault rupture deformation is analyzed. A detailed model is employed for the aforementioned fault rupture soil–foundation–structure interaction (FR-SFSI), with the superstructure modeled in a simplified manner: the pier, of height H_p and stiffness EI_p, is included in the model; the bridge deck is replaced by equivalent lateral and rotational springs, K_x and K_θ, respectively. For the case of a continuous deck monolithically connected to piers, K_x represents the axial stiffness of the deck and K_θ the bending stiffness of the pier-deck connection. Correspondingly, for a seismically isolated bridge, K_x and K_θ represent the lateral and rotational stiffness of the (elastomeric) bearings. The output of this step is dual: (i) it provides information regarding the distress of the foundation system (e.g. the internal forces in piles, in case of a piled foundation); and (ii) it provides the necessary input for the second step, the horizontal and

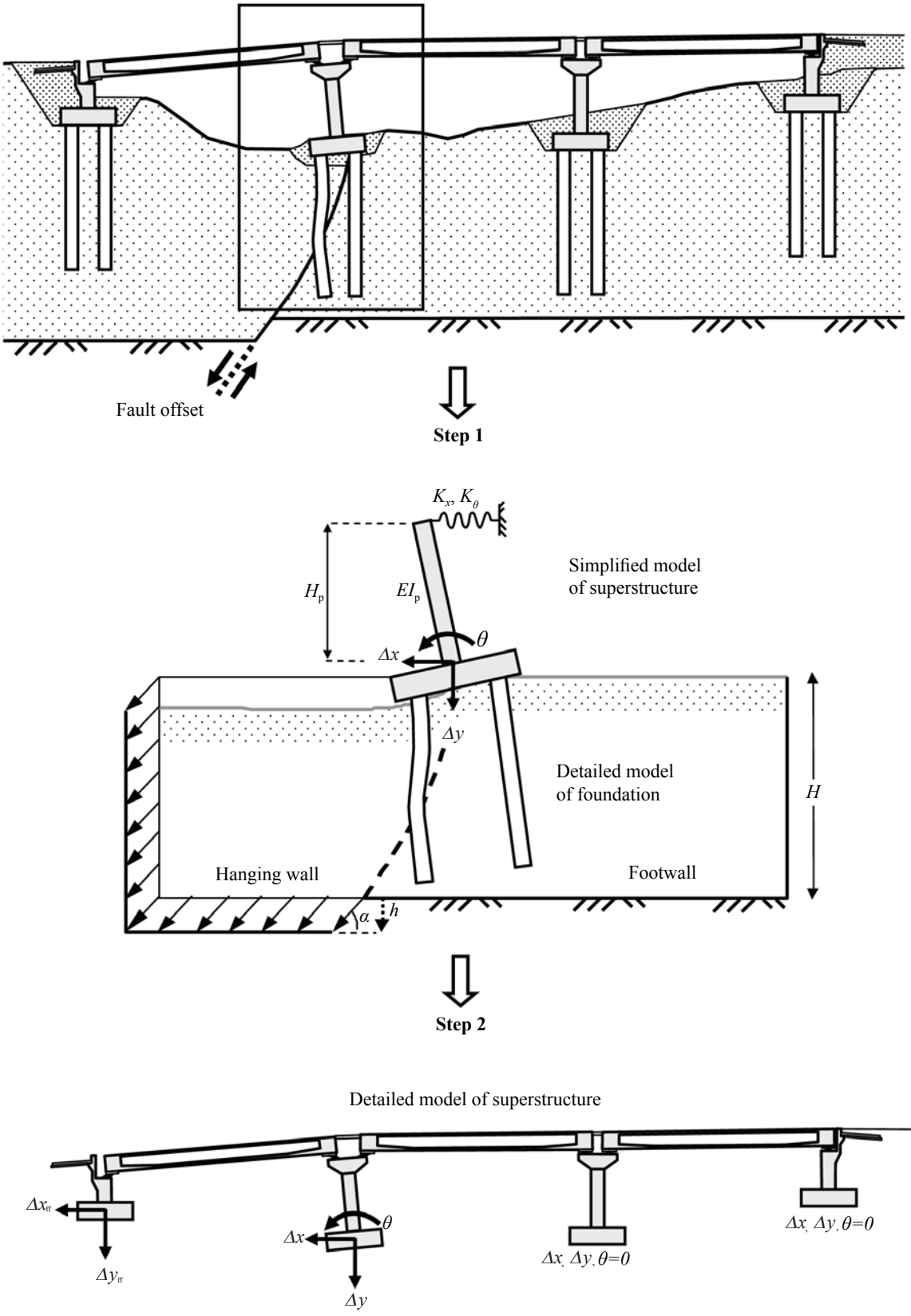

Fig. 3 Problem definition and analysis methodology. The analysis of the soil–structure system subjected to faulting-induced deformation is conducted in two steps. In Step 1, we analyze the response of a single bridge pier subjected to fault rupture deformation. A detailed model is employed to model fault rupture soil–foundation–structure interaction (FR-SFSI), with the superstructure modeled in a simplified manner. In Step 2, the detailed model of the superstructure is subjected to the computed displacements and rotations of Step 1

vertical displacements Δx and Δy and the rotation θ at the base of the pier.

In Step 2 (*global* level), the detailed model of the superstructure is subjected to the computed Δx , Δy , and θ from Step 1.

Following a worldwide overview, bridge systems were categorized according to their geometric characteristics, the typology of their superstructure, and their foundation. Based on this, and aiming to render the results of this research as general as possible, two generalized bridge types were selected: (i) a typical 350 m long viaduct bridge (Fig. 4), and (ii) a typical 75 m long 3-span overpass bridge (Fig. 5). For each bridge type, alternative superstructure typologies were investigated.

As shown in Fig. 4, five different alternatives were investigated for the typical viaduct:

(a1) a 7-span viaduct, with continuous deck monolithically connected to piers;

(a2) the same system, but the deck supported through elastomeric bearings;

(a3) 7 simply supported decks on elastomeric bearings;

(b1) a 5-span viaduct, with continuous deck monolithically connected to piers; and

(b2) same system, but the deck lying on elastomeric bearings.

For these alternatives to be realistic, the deck of the 7-span viaduct is assumed to be different from that of the 5-span alternative: a large box section of sectional stiffness EI_d = 2000 GNm^2, adequate for cantilever construction of the 87.5 m span; and a small box section of sectional stiffness EI_d = 100 GNm^2, adequate for standard construction of the 50 m spans. The bridge piers are also typical for each alternative, with their sectional stiffness EI_p varying with the pier height H_p, so that the member stiffness of each pier K_p is kept constant: a commonly used rule in practice. The value of K_p was computed based on the mass of the deck m_d, so that the dominant period T of each system corresponds to realistic values: T = 1.0 s for alternative (a1); and T = 1.5 s for alternative (b1). For the seismically isolated alternatives (a2, a3, and b2), the stiffness of the elastomeric bearings was computed so that T = 3.0 s.

Two alternatives were selected for the typical overpass bridge (Fig. 5):

(a) a three-span continuous deck monolithically connected to piers; and

(b) three simply supported decks on elastomeric bearings.

As in the previous case, the two alternatives were selected to correspond to realistic bridges. Since the span is now smaller (25 m), an even smaller box section of EI_d = 60 GNm^2 was selected. The cross-sectional stiffness of the bridge piers was set to EI_p = 20 GNm^2. Thus, in combination with the mass of the deck, m_d = 800 Mg, the non-isolated system would have a fundamental vibration period T = 0.5 s in the longitudinal direction, a rather typical value. For both alternatives, the stiffness of the elastomeric bearings was selected to achieve T = 2.5 s.

As depicted in Figs. 4 and 5, for each bridge type, different scenarios were investigated with respect to the location of fault outcropping. The first set (in grey) assumes fault rupture emergence between two consecutive piers and the second (in black) refers to the case of the dislocation taking place at the location of a pier. In the first case, the input to the detailed bridge model (of Step 2) only includes the displacements Δx and Δy, and the interaction analysis of Step 1 is redundant. In the second case (rupturing at the location of a pier), the FR–SFSI analysis is mandatory to compute Δx and Δy (which are affected substantially by the presence of the pier foundation), and the input to the Step 2 model also includes the rotation θ at the base of the pier, which is equally (if not even more) important to Δx and Δy, especially for tall piers. At the foundation level, an adequate number of *local* rupture location scenarios were parametrically investigated. For the input to the subsequent bridge superstructure analysis (Step 2), the worst-case *local* rupture location scenario was employed.

Since the response of the bridge system largely depends on the response of its foundation to the imposed tectonic dislocation, a number of typical foundation systems were parametrically investigated in the first analysis step. As for the superstructure, realistic foundation systems were selected for analysis, corresponding to the parametrically analyzed bridge types (Figs. 4 and 5). The idealized foundation types shown in Fig. 6 were selected for analysis:

(i) a "small" 2 × 4, d = 1.0 m, L = 15 m pile group, suitable for the overpass bridge;

(ii) a "large" 3 × 3, d = 1.5 m, L = 15 m pile group, suitable for the 7-span viaduct bridge;

(iii) a "small" 5 m × 5 m × 10 m (width × length × depth) caisson foundation, suitable for the 7-span viaduct); and

(iv) a "large" 10 m × 10 m × 15 m (width × length × depth) caisson foundation, suitable for the 5-span viaduct.

In all cases, different scenarios were investigated with respect to the soil conditions, with Layer 1 ranging from idealized loose to dense sand (Anastasopoulos *et al*., 2007), and Layer 2 (for the piled foundations) ranging from dense sand to rock-type material. Thus, both floating (with the material of Layer 2 being the same with Layer 1) and end-bearing piles (with the material of Layer 2 being substantially stiffer than Layer 1) were investigated. As discussed previously, for each foundation system, an adequate number of *local* fault rupture location scenarios were investigated.

The following section discusses the finite element (FE) analysis method employed for FR–SFSI analysis at the *local* pier-foundation level (Step 1). Then, the key findings concerning the response of piled and caisson

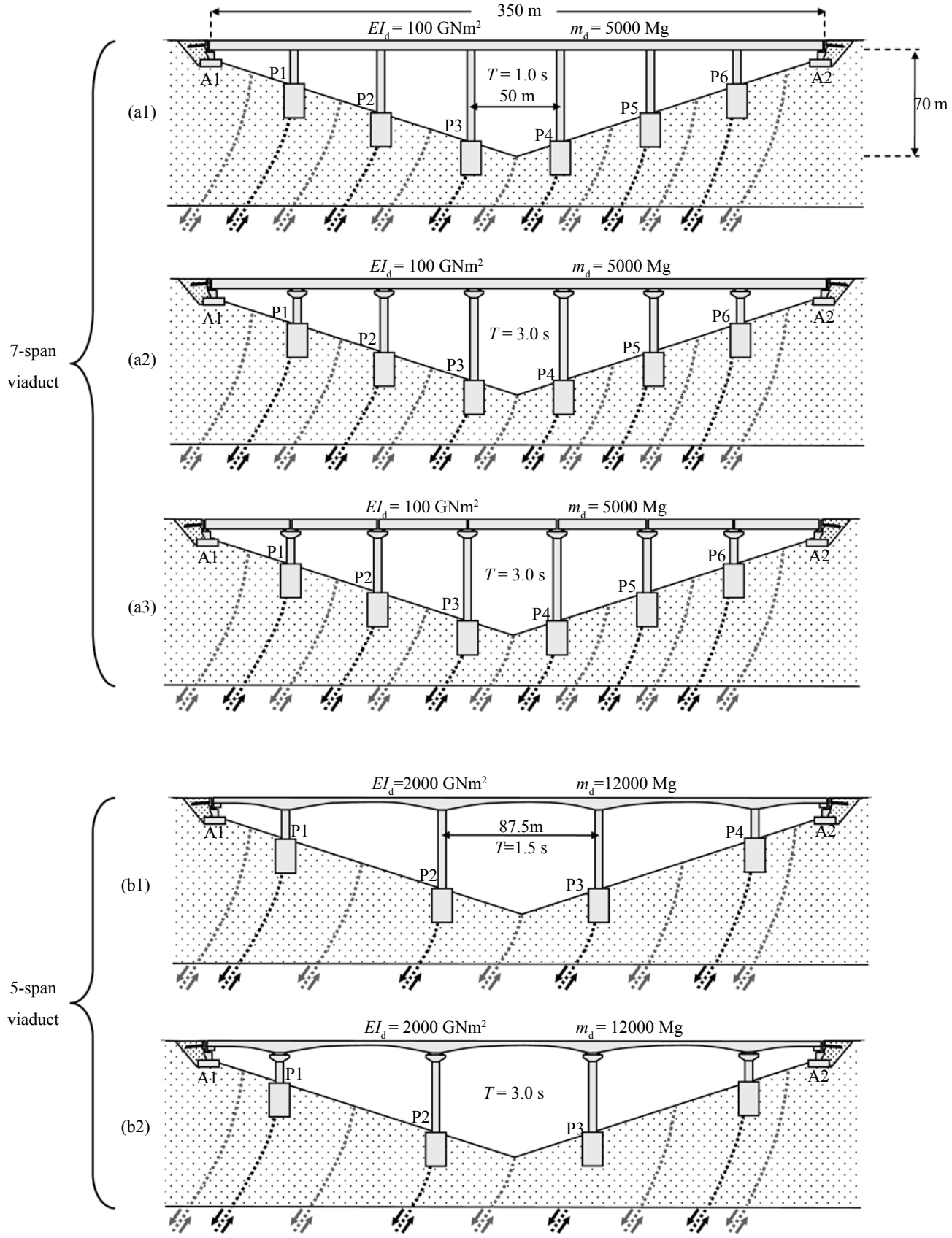

Fig. 4 Parametrically investigated viaduct bridges : (a1) 7-span viaduct, continuous deck monolithically connected to piers ; (a2) same system, but deck supported through elastomeric bearings; (a3) 7 simply supported spans on elastomeric bearings ; (b1) 5-span viaduct, continuous deck monolithically connected to piers ; and (b2) same system, but deck on elastomeric bearings

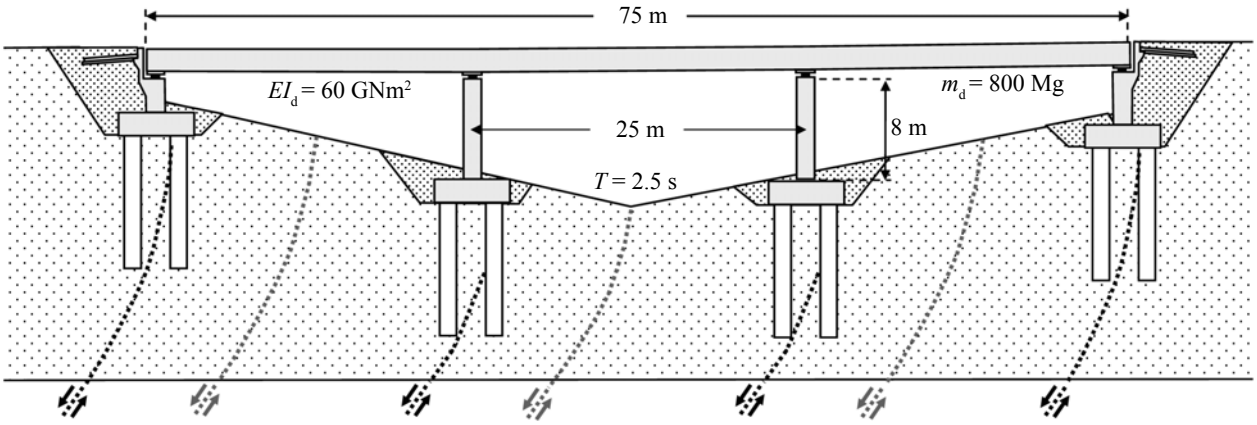

(a) continuous deck supported on elastomeric bearings

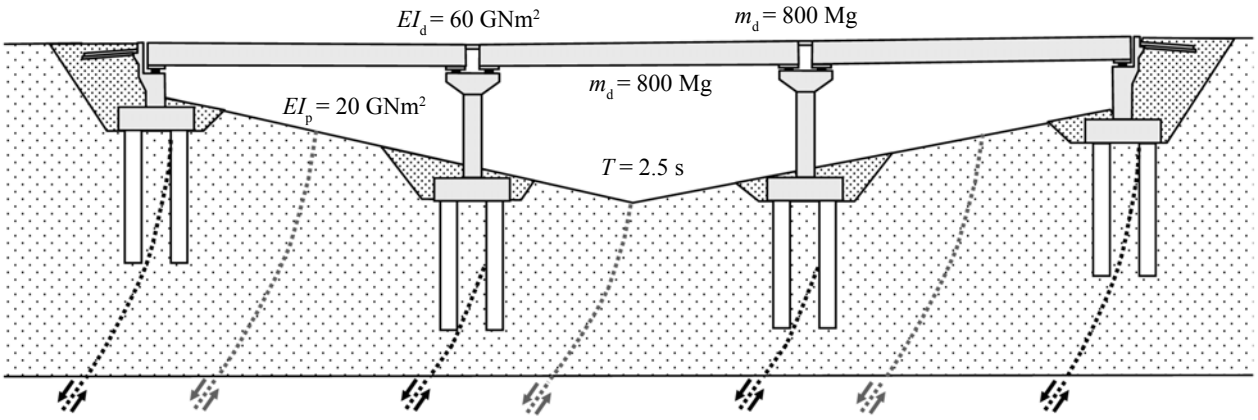

(b) 3 simply supported spans on elastomeric bearings

Fig. 5 Parametrically investigated typical 3-span overpass bridges

foundations are discussed, followed by the main results of the *global* analysis of the superstructure (Step 2).

3 Finite element analysis method

To realistically model the response of piled and caisson foundations, the analysis is conducted in 3-D. Utilizing the FE code ABAQUS, the soil is modeled with hexahedral (8-node) brick-type elements of dimension d_{FE} = 1 m to achieve a reasonably refined mesh, as documented in detail in Anastasopoulos *et al*. (2007).

In the case of caisson foundations, the mesh is made sparser far from the area of interest. The caisson is also modeled with brick-type elements, which are assumed to be linear elastic: E = 25 GPa (concrete). Following the results of an initial sensitivity study, the total width of the model was set to $B = 3H$. Although this is less than the $B = 4H$ recommendation of Bray (1990) and Bray *et al*. (1994a; 1994b), the sensitivity analysis showed that the results of interest were hardly affected, while the computational time was reduced substantially. Hence, it was accepted as a reasonable compromise. The superstructure is taken into account, as described previously (see also Fig. 3). The pier is modeled with beam elements and the deck with appropriate grounded springs. In all cases, half of the foundation system is analyzed, taking advantage of problem symmetry.

In the case of piled foundations, the mesh is refined further close to the area of the piles ($d_{FE} \approx 0.25$ m) to correctly capture their geometry. Due to this necessary refinement, and to complete this research within the requested time frames, the width of the model was further reduced to $B = 2.5H$. "Dummy" (i.e. of zero mass and stiffness) brick-type elements are used to model the geometry of the piles. The piles are actually modeled with beam elements, rigidly connected to the peripheral nodes of the corresponding dummy elements. This way, soil-to-pile interaction is modeled realistically, and contact is attained on the actual periphery of the pile and the actual pile tip area. The piles are connected to a rigid pile cap, which is modeled with hexahedral brick-type elements. Both the piles and the pile cap are assumed

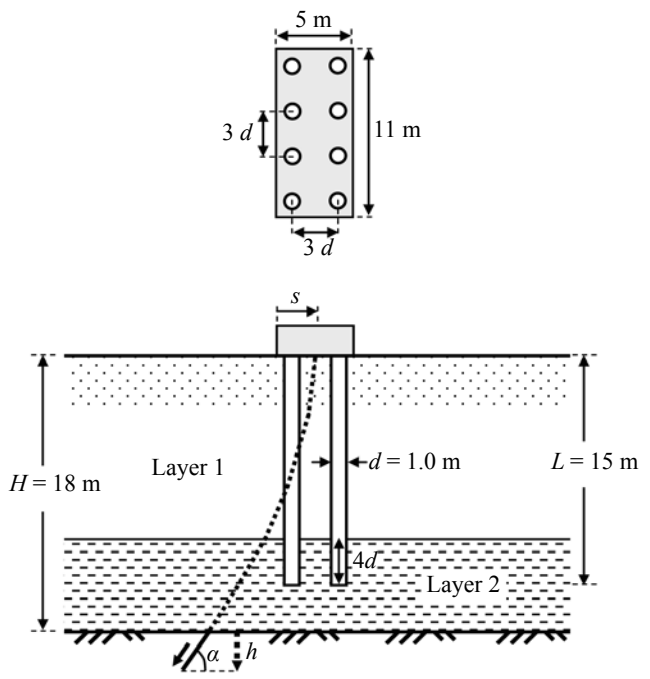

(a) 2 × 4, d = 1.0 m, L = 15 m pile group (suitable for the overpass bridge)

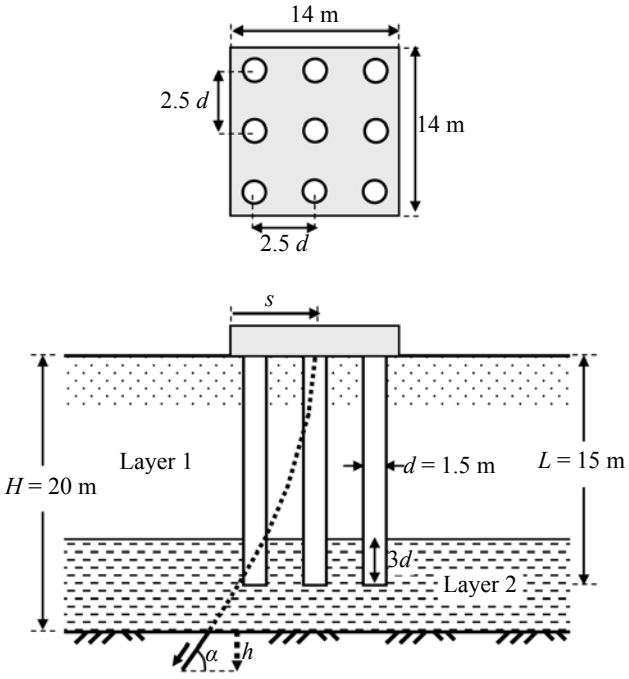

(b) 3 × 3, d = 1.5 m, L = 15 m pile group (suitable for the 7-span viaduct bridge)

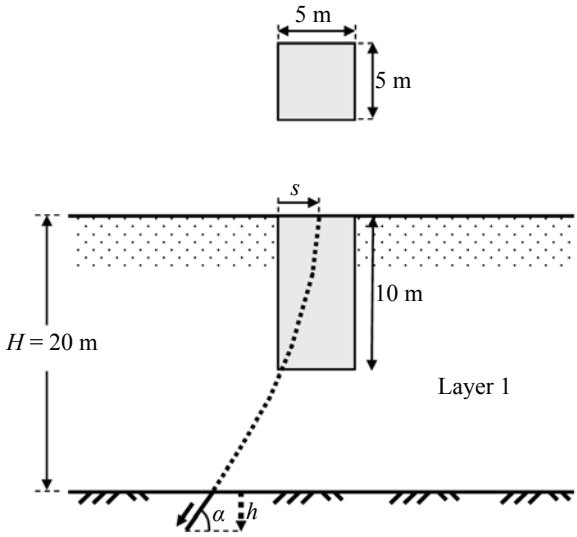

(c) Small 5 m × 5 m × 10 m caiss on foundation (suitable for the 7-span viaduct)

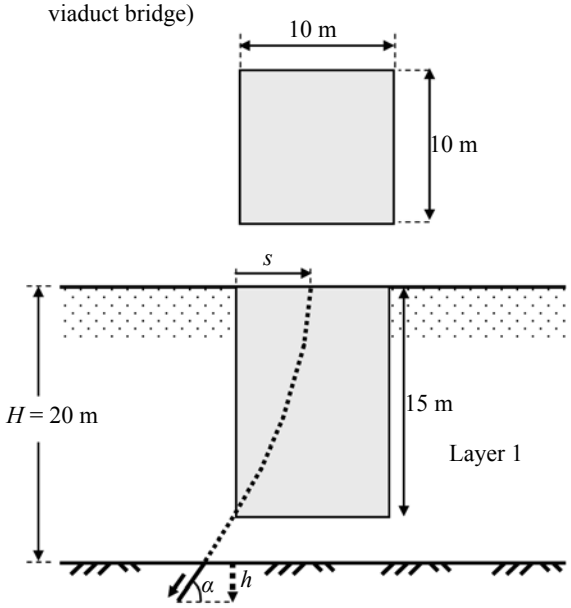

(d) Large 10 m × 10 m × 15 m caisson foundation (suitable for the 5-span viaduct

Fig. 6 Parametrically investigated foundation systems

linear elastic, with E = 25 GPa (concrete).

The analysis is performed in two steps. First, fault rupture propagation through soil is analyzed in the free field, ignoring the presence of the foundation (pile group or caisson). Then, knowing the location of fault rupture emergence, the foundation is positioned so that the unperturbed rupture outcrops at distance s from its hanging wall (left) edge (see Fig. 6). In the case of the "small" 2 × 4 pile group, five scenarios were parametrically investigated with respect to the location of fault outcropping: s = 2, 5, 7, 8, 9, 10, and 11 m. Observe that although the width of the pile-cap is 5 m, due to the non-vertical propagation of the rupture larger values of s are required to cross the pile group at all possible locations. Similarly, for the "large" 3 × 3 pile group, s = 3, 7, 11, 15, 16, and 20 m; for the "small" 5m × 5m × 10m caisson, s = 2, 4, and 8 m; and for the large 10m × 10m × 15m caisson, s = 1, 5, 9, 13, 14, and

18 m.

Soil behavior is modeled with an elastoplastic constitutive model with a Mohr-Coulomb failure criterion and isotropic strain softening, encoded in ABAQUS through a user subroutine. Strain softening is introduced by reducing the mobilized friction angle φ_{mob} and the mobilized dilation angle ψ_{mob} with the increase of plastic octahedral shear strain. Soil behavior before yielding is modeled as linear elastic. Model parameters are calibrated through direct shear test results, and an approximate scaling method is employed to take account of scale effects. Two idealized soil materials and a simplified rock-type material are utilized in the analysis:

- Loose Sand: $\varphi_p = 32^o$, $\varphi_{res} = 30^o$, $\psi_p = 3^o$, $\gamma_y = 0.030$, $\gamma_p^p = 0.06$, and $\gamma_f^p = 0.0616$
- Dense Sand: $\varphi_p = 45^o$, $\varphi_{res} = 30^o$, $\psi_p = 18^o$, $\gamma_y = 0.015$, $\gamma_p^p = 0.05$, and $\gamma_f^p = 0.0516$
- Rock-type material: $\varphi_p = 37^o$, $\varphi_{res} = 25^o$, $\psi_p = 15^o$, $\gamma_y = 0.002$, $\gamma_p^p = 0.02$, and $\gamma_f^p = 0.0205$

where γ_y is a parameter associated with the initial "elastic" response of the soil material, γ_p^p the plastic shear strain at peak conditions, φ_{res} the residual value of the friction angle, ψ_p the ultimate dilation angle, and γ_f^p the plastic octahedral shear strain at the end of softening (Jewel and Roth, 1987; Gerolymos *et al*., 2008).

The FE modeling methodology employed herein has been extensively validated through: (a) *qualitative* comparisons with numerous published experimental data (Horsfield 1977; Cole and Lade, 1984) and earlier case histories (Slemmons, 1957; Brune and Allen, 1967; Taylor *et al*., 1985); (b) *semi-quantitative* comparisons with case histories from the 1999 earthquakes of Kocaeli and Turkey (Anastasopoulos & Gazetas, 2007a,b; Faccioli *et al*., 2008); and (c) through *quantitative* blind predictions of centrifuge model tests (Anastasopoulos *et al*., 2008).

4 Piled foundations

Although piled foundations are used to protect the superstructure by minimizing the settlements and the dynamic (shaking-induced) rotations, their performance to concentrated deformation is not always beneficial. Evidence from recent earthquakes has implicated the piles for the observed structural damage. The previously discussed failure of several piles of the Bolu Viaduct in the second 1999 Turkey earthquake is definitely one such case. Another example is the damage of the pile-supported Attatürk Stadium in Denizerler during the earlier 1999 Kocaeli earthquake.

This section discusses the key findings of the parametric analysis at the *local* foundation level for the case of piled foundations. The detailed presentation of all analysis results is out of the scope of this paper. Hence, we focus on characteristic results that provide insight to the governing interaction mechanisms.

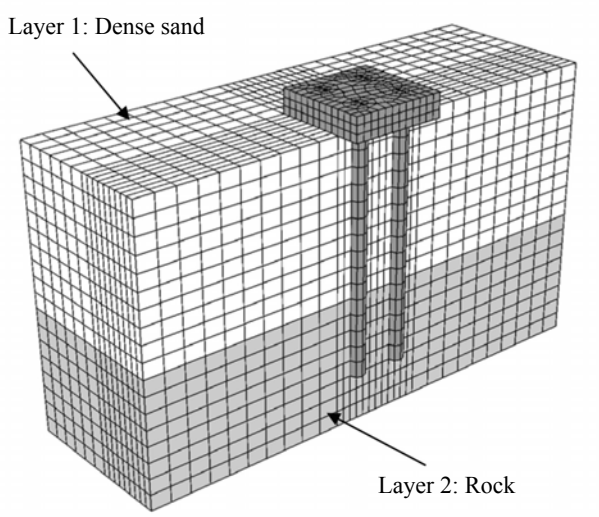

Fig. 7 Finite element mesh for the case of the 2 x 4 pile group. Half of the pile group is analysed, taking advantage of problem symmetry. The first row of elements are removed in the plot to show the first row of piles

4.1 "Small" 2 × 4 pile group

The response of the "small" 2 × 4 pile group was analyzed first, which is adequate for the typical overpass bridge (Fig. 7). Layer 1 is assumed to be the idealized dense sand and Layer 2 is the idealized rock-type material — the case of end-bearing piles. The vertical superstructure load transmitted onto the group is equal to $V = 2500$ kN, typical of an overpass bridge. The role of the superstructure is modeled in a simplified manner, as illustrated in Fig. 3.

Figure 8 portrays the response of the pile group subjected to $h = 0.05$ m normal faulting at distance $s = 5$, 7, 8, and 10 m, in the form of FE deformed mesh with superimposed plastic strain. The selection of such a small imposed bedrock dislocation is deliberate, to clearly demonstrate the sensitivity of pile foundations to this type of loading. As seen in Fig. 8(a), for $s = 5$ m (i.e. the unperturbed fault rupture would outcrop near the right edge of the pilecap), the pile group "forces" the dislocation to divert towards the hanging wall (to the left side). As a result, the foundation is not subjected to substantial deformation. Bending moments do not exceed 600 kNm (with a "heavy" reinforcement ratio, the ultimate design capacity M_{ult} of the $d = 1.0$ m piles could reach 3000 kNm), but the pile group remains practically intact. Observe also that the pilecap is not subjected to any measurable displacement or rotation.

Moving the fault rupture at $s = 7$ m (i.e. in the free-field, the fault would have emerged 2 m to the right of the footwall edge of the pilecap), the response of the group dramatically worsens (Fig. 8(b)). Now, a rather distinct bifurcation of the dislocation takes place,

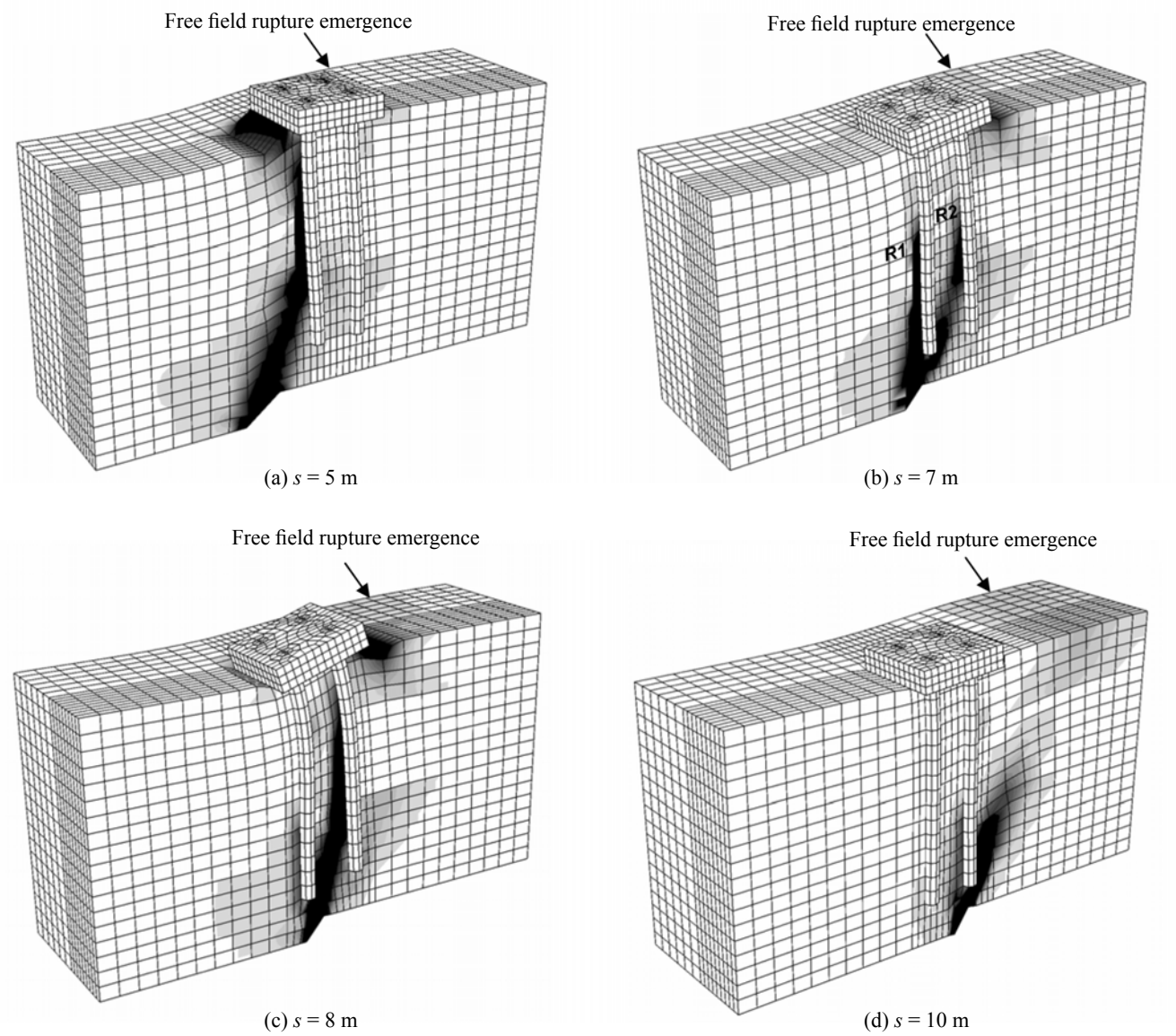

Fig. 8 FE deformed mesh with superimposed plastic strain contours for the 2 × 4 pile group, subjected to h = 0.05 m normal faulting (deformation scale factor = 40) : (a) s = 5 m, (b) s = 7 m, (c) s = 8 m, and (d) s = 10 m

leading to development of two separate ruptures: the first one, *R1*, is diverted by the first row of piles towards the hanging wall (left); and the second, *R2*, outcrops between the two rows of piles. As a result, the front row of piles (left) is being "pulled" outwards (to the left) and downwards by the moving hanging wall, while the back row (right) cannot follow as it lies on the footwall. This imposed differential displacement of the two pile rows, in combination with the kinematic restraints of the pilecap, leads to development of rather large bending moments on the order of 1500 kNm. Furthermore, pilecap displacement and rotation is now discernible.

The distress of the pile group is largest for s = 8 m (Fig. 8(c)). In contrast to the previous case, the dislocation now just misses the tip of the front pile row. Paradoxically, this small "detail" worsens the response of the soil-foundation system to a rather large extent. While in the previous case (s = 7 m), the rupture experienced bifurcation and diffusion as it interacted with the first pile row, now such stress-relieving phenomena cannot develop and the rupture is left "free" to develop to its full extent between the two pile rows. Hence, the two rows suffer the largest differential displacement, which leads to bending moments M of the order of 2800 kNm (i.e. M almost reaches M_{ult}) and measurable displacement and rotation of the pilecap. It would be interesting to think of this case in reality: while for an observer at the ground surface the rupture would appear to have missed the foundation, due to its non-vertical propagation path it would have intersected with the two pile rows, causing substantial pile distress and rotation of the superstructure.

Moving the fault rupture to s = 10 m (Fig. 8(d)) leads to less stressing of the piles. Now, the propagating rupture plane intersects the tip of the back row of piles, undergoes substantial diffusion and limited local

bifurcation. Both pile rows are lying on the hanging wall, being subjected to almost the same horizontal and vertical displacements. As a result, they are not subjected to substantial differential displacements, and consequently the tectonically-induced M does not exceed a mere 300 kNm. The rotation of the pilecap, which is directly related to the differential displacement between the pile rows, is insignificant. In stark contrast, since the whole pile group is moving along with the hanging wall, horizontal and vertical displacements at the pier base are substantial.

Figure 9 illustrates the distribution along the depth of pile bending moments M and axial forces N for the worst-case scenario (s = 8 m). The net stressing due to the faulting-induced deformation is shown (i.e., the stressing due to dead loads has been subtracted). For both rows, the largest M is at the connection with the pilecap. As expected, being pulled downwards, the hanging wall side piles (pile 1) develop tension ($N \approx$ 2500 kN). The footwall side piles (pile 2), lying on the footwall resist such imposed deformation; they naturally develop compression ($N \approx$ –5500 kN). The largest compression is at the soil-rock interface (at 12 m depth). Interestingly, the largest tension of pile 1 is a few meters higher (at about 10 m depth). This is attributable to the rupturing–induced plastification of the rock (layer 2) close to the pile tip.

Figure 10 produces a synopsis of the results, emphasizing the effect of the location s of fault outcropping to: (a) the horizontal Δx and vertical Δy displacement at the pier base, (b) the rotation θ at the pier base, (c) the maximum and minimum bending moments M of the piles, and (d) the maximum and minimum axial forces N of the piles. One would have expected that Δx and Δy would increase with s. As the location of the rupture moves to the right, the pile group tends to be more on the hanging wall, and is thus subjected to larger displacements. However, Δx and Δy at the pier base are also related to the rotation θ of the pilecap. The latter is directly related to the differential displacement between the two rows of piles, and is thus maximum for s = 8 m. As a result, Δy at the pier base is also largest for the same rupture location. On the other hand, Δx is not affected to the same extent by θ, being

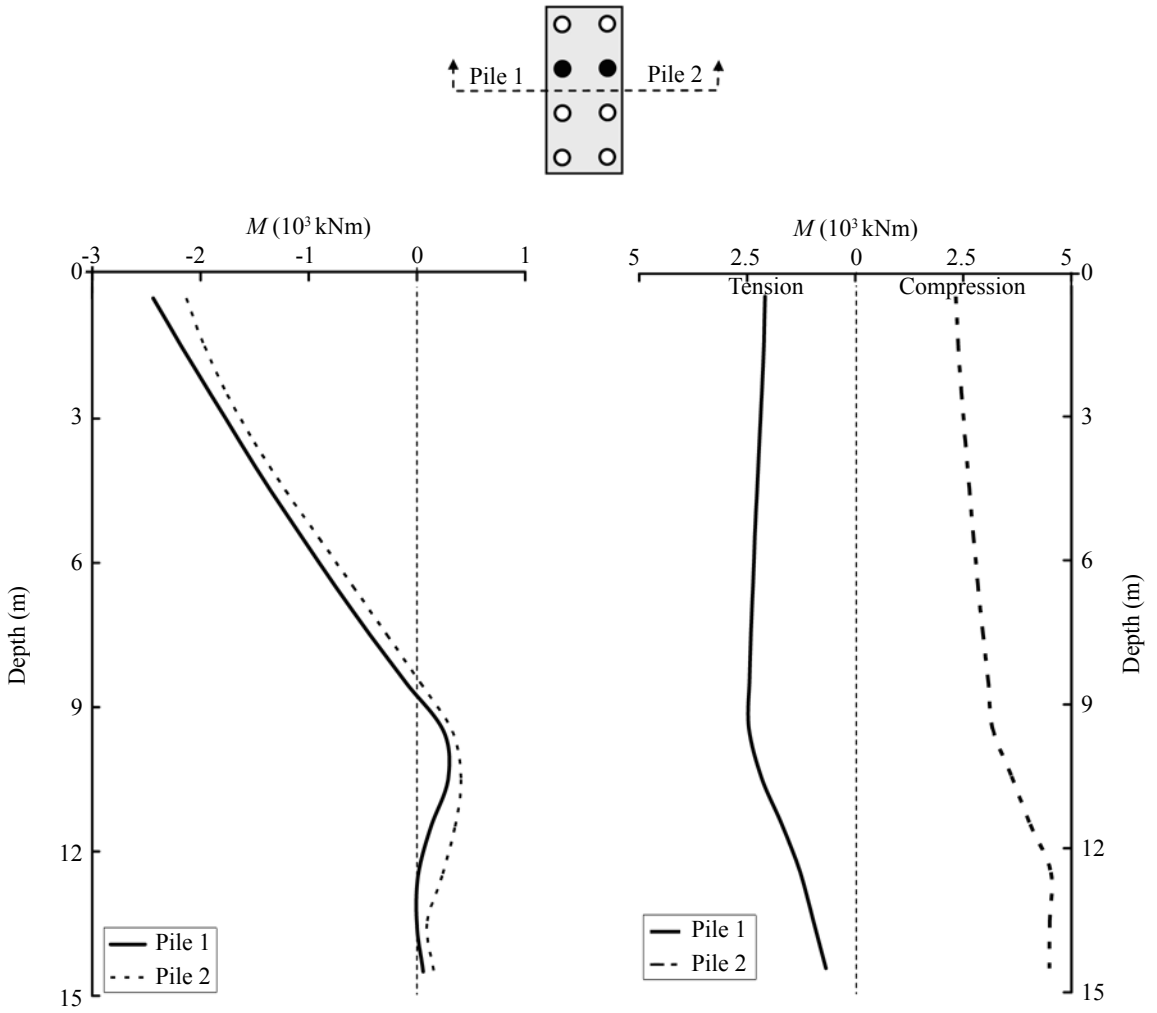

Fig. 9 Pile bending moment and axial force for the 2 x 4 pile group, subjected to normal faulting at s = 8 m, h = 0.05 m

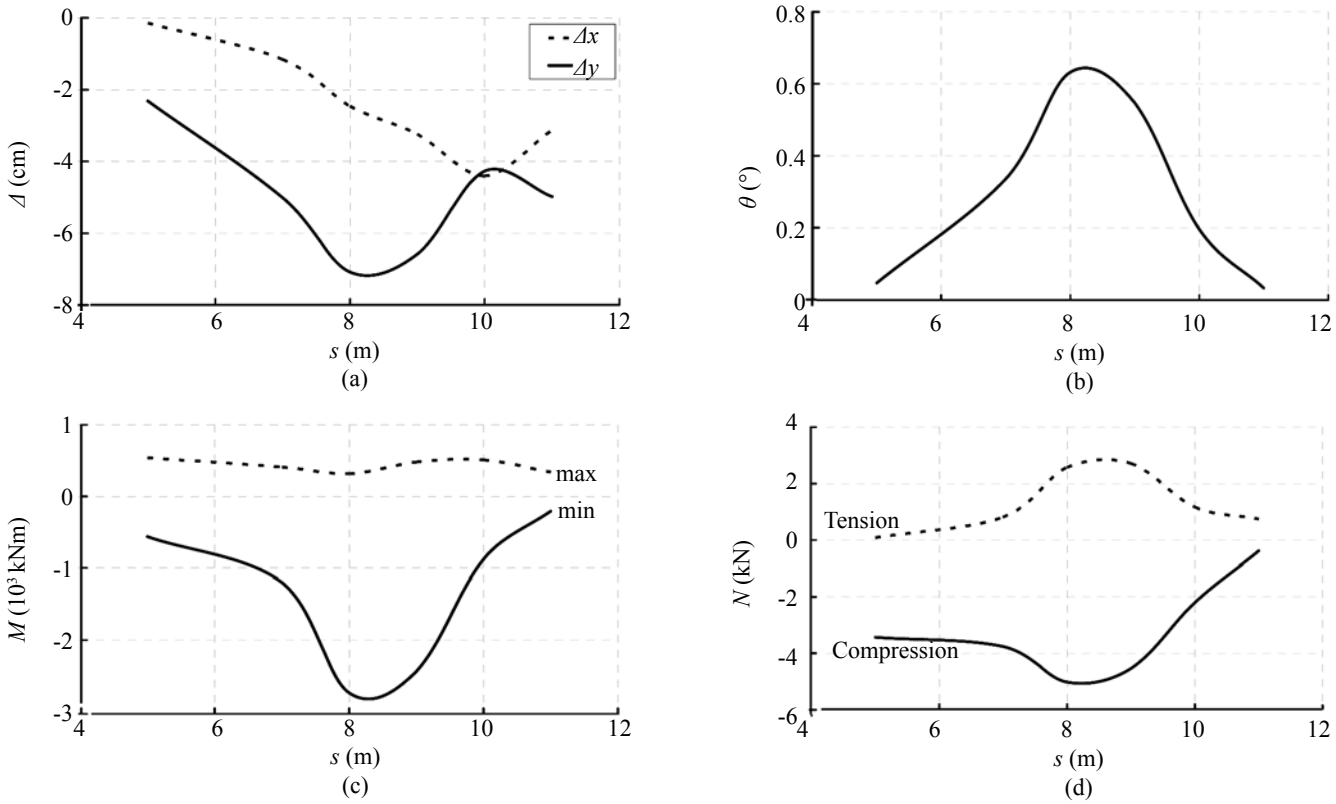

Fig. 10 Synopsis of analysis results for the 2 x 4 pile group, h = 0.05 m. Effect of the location s of fault outcropping to: (a) Horizontal Δx and vertical displacement Δy at the pier base; (b) Rotation θ at the pier base; (c) Maximum and minimum bending moment M of the piles and (d) Maximum and minimum axial force N of the piles

maximum for s = 10 m. Being the direct result of the differential displacement between the two pile rows, the stressing of the piles (exhibited through M and N) is also largest for s = 8 m (i.e. when the rupture outcrops exactly between the two rows).

In summary, it has been shown that a rather minor bedrock offset (h = 0.05 m in the case examined herein) is enough for typical end-bearing piles to reach their ultimate structural capacity, even in case of very "heavily" reinforced piles.

4.2 "Large" 3 × 3 pile group

This section deals with the "large" 3×3 pile group, which would be a reasonable solution for the 7-span viaduct. Since the response of end-bearing piles has already been shown to be rather problematic, the focus here is on the response of floating piles (i.e. Layer 2 being the same with Layer 1). The soil is assumed to be idealized dense or loose sand. The vertical superstructure load transmitted onto the pile group is assumed to be equal to 7000 kN, typical for a 7-span viaduct.

To illustrate the effect of soil resilience, the response of the pile group was compared in dense and loose sand. Fig. 11 depicts the evolution of M with the increase of imposed bedrock offset h for a normal faulting at distance s = 11 m (representing the worst-case scenario). In dense sand, all piles are subjected to substantial bending, with the hanging wall side piles (pile 1) being stressed the most and the footwall side piles (pile 3) the least. Soil resilience is clearly beneficial in terms of pile stressing, since in loose sand, the maximum M is a little more than merely one third of that of dense sand. Naturally, such large bending moments would exceed the ultimate capacity, M_{ult}, of the d = 1.5 m piles. With a very "heavy" reinforcement ratio on the order of 4%, M_{ult} would be of the order of 8000 kNm. This means that in dense and stiff soil, the hanging wall side piles (pile 1) would be the first to fail, at h = 0.35 m, followed by the medium row (pile 2), at h = 0.52 m, and finally the footwall side row (pile 3), at h = 1.61 m. In stark contrast, in loose sand, only the first row (pile 1) would fail, and for substantially larger imposed deformation: h = 0.93 m. Note also that while at the early stages of deformation (h < 0.3 m) the stressing of the three pile rows is qualitatively similar to the case of dense sand (pile 1 is stressed the most; pile 3 the least), the increase of the imposed deformation leads to a mechanism change: where the footwall side piles (pile 3) experience more stressing than the medium row (pile 2).

The demonstrated beneficial role of soil resilience (comparing the idealized dense with the idealized loose sand) is as follows:

(a) *Quasi-elastic* behavior: Before the soil surrounding the piles starts to yield, the decrease of soil stiffness leads to an increase of the relative pile stiffness,

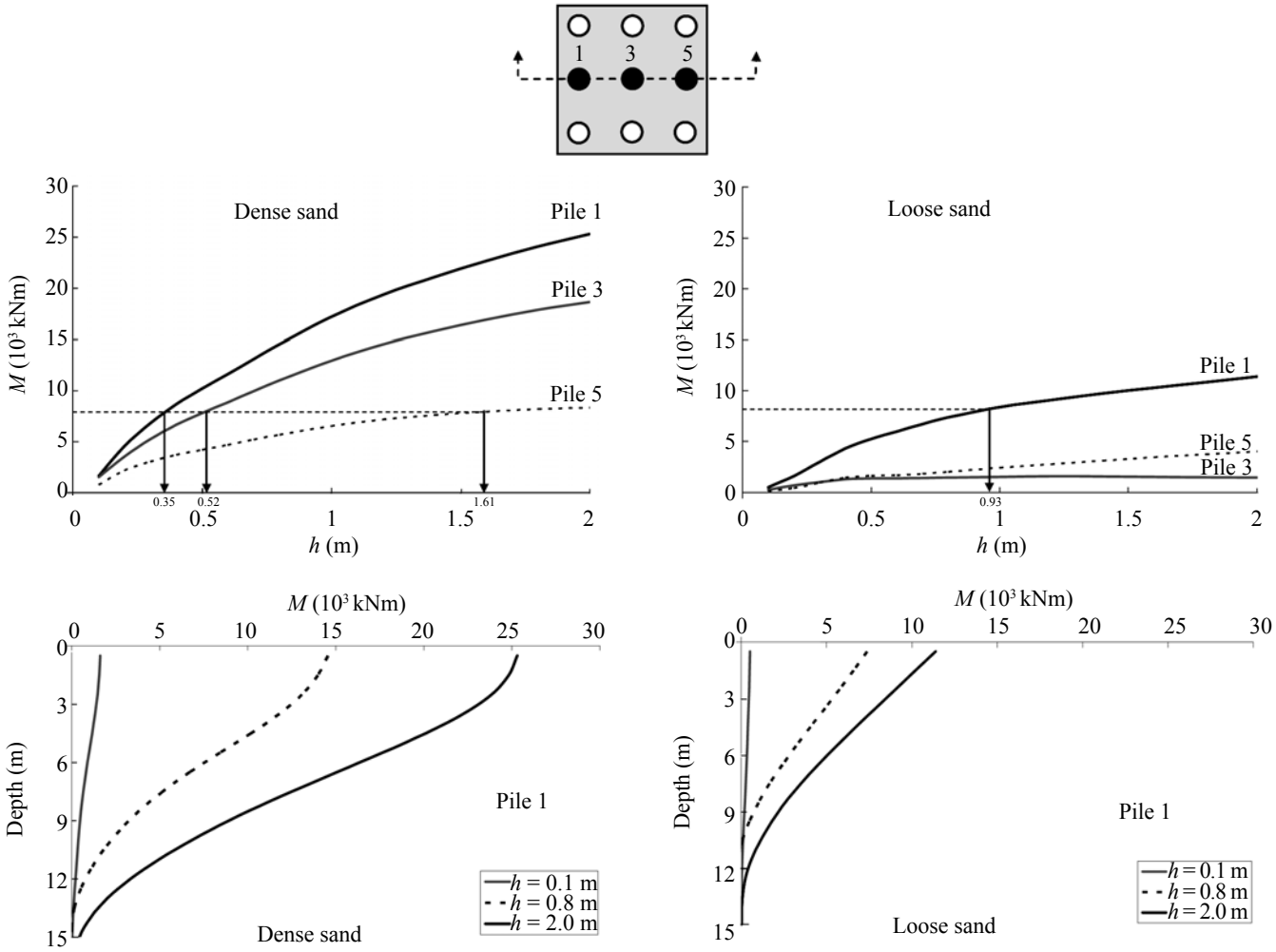

Fig. 11 Illustration of the effect of soil resilience for the 3 x 3 pile group, subjected to normal faulting at *s* = 11 m, and *h* ranging from 0.1 to 2.0 m : evolution of pile bending moments *M* with the increase of imposed bedrock offset *h* for idealized dense and loose sand

facilitating pile resistance to the imposed deformation;

(b) *Plastic* behavior: The decrease of soil strength ($\varphi_p = 45^o$ in dense sand; $\varphi_p = 32^o$ in loose sand) speeds up soil failure at the pile-soil interface, allowing the piles to sustain larger imposed deformation before reaching structural failure. Stress relieving phenomena, such as fault rupture diversion and bifurcation, and diffusion of plastic deformation are also facilitated; and

(c) *Post failure* behavior: After the soil at the pile-soil interface has reached failure, the decrease of soil dilatancy ($\psi_p = 18^o$ in dense sand; $\psi_p = 3^o$ in loose sand) leads to a substantial decline of the rate of increase of pile stressing with the imposed deformation *h*. Observe in Fig. 11, that while in dense sand the evolution of pile stressing with *h* exhibits a hardening-like behavior, in loose sand it resembles an elastic-perfectly plastic one.

These three reasons are also responsible for the superior performance of floating piles (this group) compared to end bearing piles (2×4 pile group). While only 5 cm of bedrock offset was enough for *all* of the *d* = 1.0 m end-bearing piles to reach structural failure, in dense sand the first row of the *d* = 1.5 m piles sustained 35 cm before reaching failure; the other two rows have even larger safety margins (0.52 m and 1.61 m). Analyses (not shown herein due to space limitations) of the 3×3 pile group with Layer 2 being changed to the idealized rock-type material confirm this conclusion. In fact, due to the disproportional increase of pile stiffness compared to M_{ult} (increasing *d* from 1.0 m to 1.5 m leads to a 500% stiffness increase, compared to a 260% increase of M_{ult}), the *d* = 1.5 m piles have even smaller safety margins if they are of the end-bearing type.

4.3 Solution: hinged pile-to-cap connection

In all cases examined, the largest pile bending moments occurred at the connection with the pilecap. This location is therefore the first candidate for plastic hinging. Preventing such failure by introducing a-priori a *hinged* pile–to–cap connection is rather intuitive.

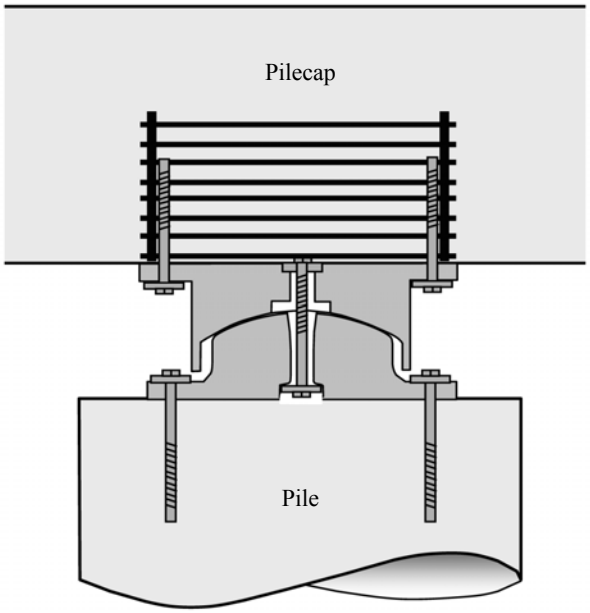

Fig. 12 Schematic drawing of a hinged pile to pilecap connection, following the concept introduced by Shimizu Co. & Kubota Co. [after Tazoh *et al*., 2002]

Furthermore, dynamic analyses (strong ground shaking, not faulting related) of pile groups have shown that the type of pile-to-cap connection greatly influences the performance of the foundation, with the hinged connection leading to substantially less pile distress, albeit at the cost of larger cap displacements and rotations compared to the traditional fixed connection (Tazoh *et al*., 2002; Gerolymos *et al*., 2008). To the best of our knowledge, the idea of a device that allows such a connection was introduced in Japan after the devastating 1995 Kobe earthquake. One such device, designed and manufactured by Shimizu Co. & Kubota Co., is schematically illustrated in Fig. 12 (after Tazoh *et al*., 2002). The cast-iron device consists of a spherical table, a spherical lid, and a high-strength bolt at the center to allow transmission of tensile forces. Shear forces are transmitted through the high-friction contact surface (spherical table–spherical lid), while almost free rotation is allowed. The performance of this device has been validated through actual scale testing, and it has been applied in practice.

To qualitatively verify the effectiveness of such a solution for the problem investigated herein, the same pile groups were re-analyzed with hinged pile-to-cap connections. Typical results are shown in Fig. 13 for the case of the 3 x 3 pile group subjected to normal faulting at s = 9 m through idealized dense sand. Evidently, due to activation of the rotational degree of freedom, the distress of all the piles is drastically reduced. Even for h = 2 m (a rather larger bedrock offset, typical of M > 7 normal fault earthquakes), M does not exceed 5000 kNm in any of the piles (Fig. 13(a)) — substantially lower than the largest possible ultimate capacity (M_{ult} = 8000 kNm) of the d = 1.5 m piles. As depicted in Fig. 13(b), due to the hinged pile–to–cap connection, the piles are now behaving like simply supported vertical beams, with M being maximum at almost the mid-height in the case of the hanging wall side row (pile 1), and at a shallower depth at the footwall side row (pile 5). The difference is clearly due to the more intense soil plastification at the

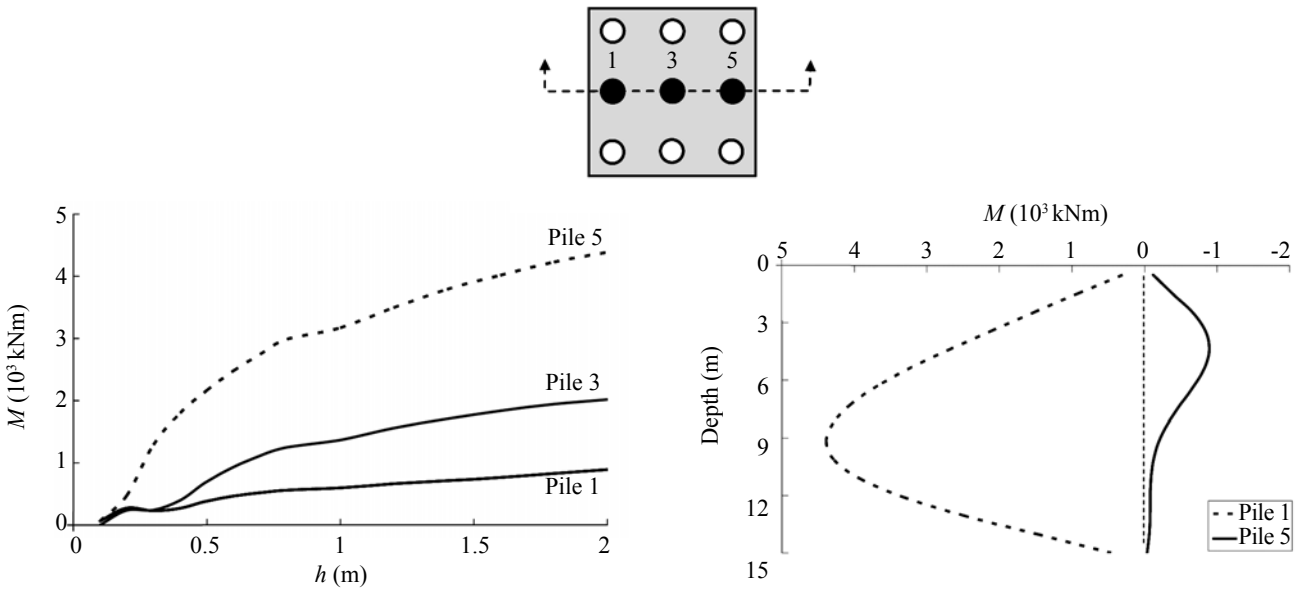

(a) Evolution of pile bending moments M with the increase of imposed bedrock offset h

(b) Distribution of pile bending moments with depth

Fig. 13 The 3 × 3 pile group equipped with hinged pile-to–pilecap connections, subjected to normal faulting at s = 11 m through idealized dense sand

front row of piles, which is more directly affected by the faulting-induced deformation.

5 Caisson foundations

The seismic performance of caisson foundations is in general considered advantageous (e.g. Gerolymos and Gazetas, 2006a,b), especially when subjected to large imposed deformation. The Kobe Ohashi (Port Island) and the Nishinomiya-Ko bridge in Kobe (Japan) partially owe their survival in the 1995 earthquake to their massive caisson foundations, which "intercepted" a substantial portion of the liquefaction–induced lateral spreading (Hanlong *et al*., 1997; Anastasopoulos *et al*., 2001). In terms of faulting–induced deformation, the Banco Central de Nicaragua constitutes one of the earliest (and one of very few) such case histories. When the strike-slip fault rupture of the 1972 M_s 6.3 Managua earthquake "attempted" to cross the Bank, thanks to the existence of a rigid reinforced-concrete caisson (the Bank's underground vault), it was diverted leaving the building totally unscathed (Niccum *et al*., 1976).

In this section, characteristic results of the parametric analysis are discussed. Due to space limitations, the focus is on the "large" 10 m × 10 m × 15 m caisson, which is adequate for the typical 5–span viaduct. Since caissons are commonly used as floating foundations, the soil is assumed to be homogenous, consisting of dense or loose sand. The vertical superstructure load transmitted onto the caisson is 20 MN, typical for the 5–span viaduct. The caisson is assumed to be fully bonded to the bearing soil — a rather conservative idealization.

Figure 14 illustrates the response of the caisson in idealized dense sand subjected to h = 2 m normal faulting at s = 1, 5, 9, and 13 m, in terms of FE deformed mesh with superimposed plastic strain. As depicted in Fig. 14(a), for s = 1 m the caisson diverts the dislocation towards the hanging wall (to the left), forming a distinct scarp at its left edge. Similarly to the case of the piled foundations, the caisson does not experience any measurable rotation or displacement.

Moving the rupture to the middle of the foundation, s = 5 m (Fig. 14(b)), leads to a more intense diversion of the rupture path, and the fault now emerges vertically along the sidewall of the caisson. The latter experiences a rotation $\theta = 1^{o}$ and measurable vertical and horizontal displacements: Δy = 0.065 m and Δx = 0.28 m. Note also the formation of a secondary antithetic rupture zone,

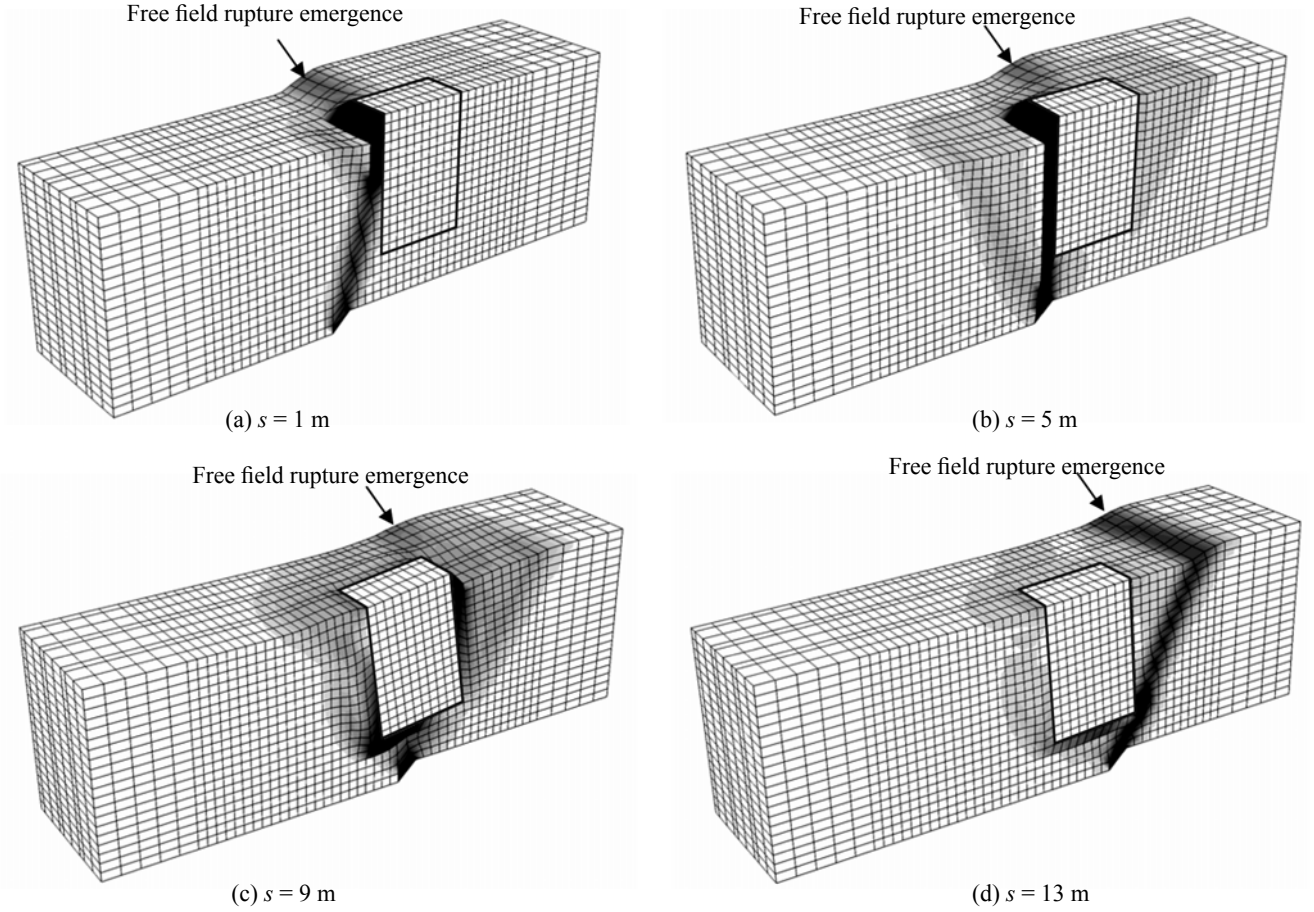

Fig. 14 FE deformed mesh with superimposed plastic strain contours for the large 10m × 10m × 15m caisson, subjected to h = 2 m normal faulting (deformation scale factor = 1) through idealized dense sand

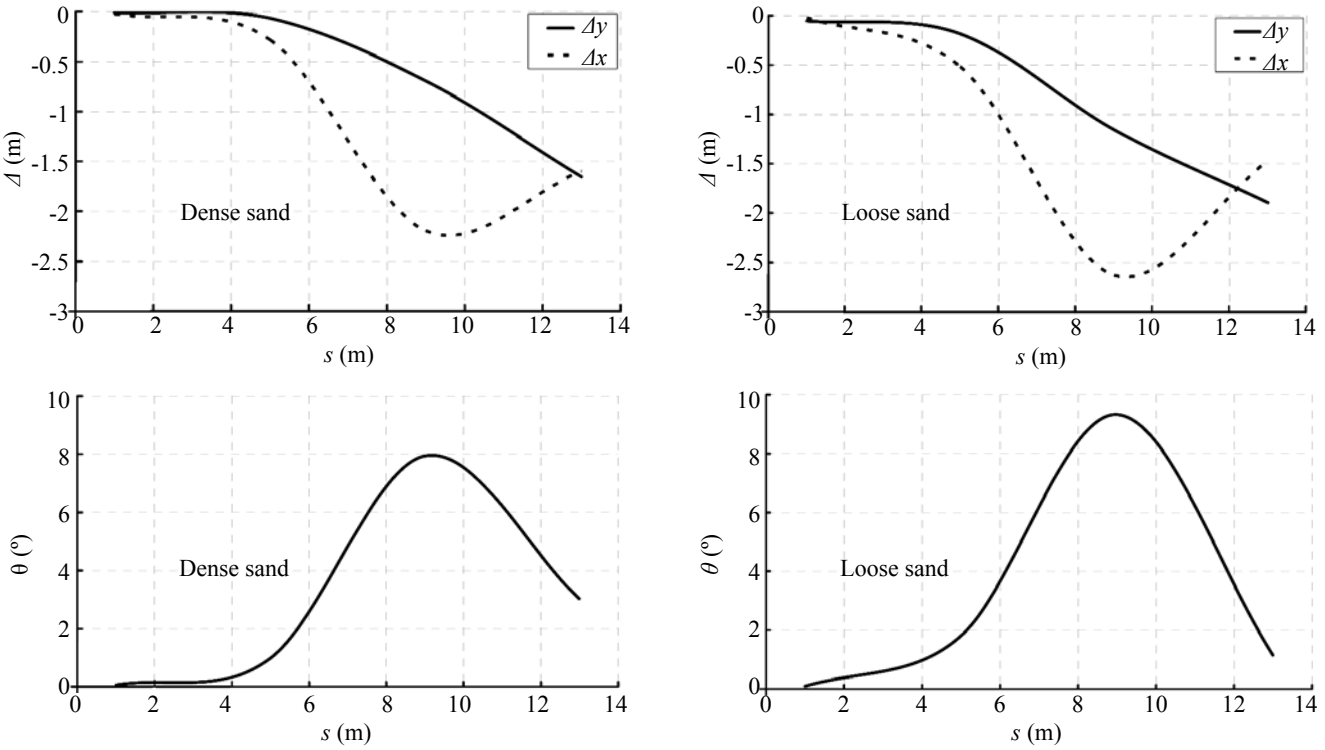

Fig. 15 Synopsis of analysis results for the 10 x 10 x 15 caisson, h = 2 m. Effect of the location s of fault outcropping and soil resilience to the horizontal Δx and vertical displacement Δy, and the rotation θ at the base of the pier

which starts propagating to the left of the main rupture at a dip angle of about 60°. Reaching the surface, in combination with the main rupture (diverted to the left edge of the caisson), it generates a gravity graben, which is a feature purely related to the kinematic constraints imposed by the rigid caisson.

For s = 9 m (Fig. 14(c)), although the imposed deformation is diffused substantially, the caisson is subjected to rather intense rotation $\theta = 8^{o}$ and substantial vertical and horizontal displacements: Δy = 0.69 m and Δx = 2.19 m. Coulomb-type active conditions are likely to form at the back (footwall side) of the caisson. Finally, for s = 13 m (Fig. 14(d)), the rupture path just intersects with the base corner of the caisson, being "defracted" towards the footwall (to the right), and finally emerging at the ground surface 8 m to the right of the footwall edge of the caisson, i.e., about 5 m to the right of its free-field outcrop location. The caisson essentially follows the movement of the hanging wall, experiencing an appreciable rotation $\theta = 3^{o}$, combined with displacements $\Delta y \approx \Delta x \approx 1.65$ m.

Figure 15 summarizes the results of this analysis, emphasizing the effect of the location s of fault outcropping and soil resilience. As for the piled foundations, Δx and Δy are in general increasing with s (as the fault rupture moves to the right, the caisson tends to be more on the hanging wall, thereby suffering larger displacements). However, Δx and Δy at the pier base are also related to θ, which is largest for s = 9 m. As a result, Δx is also maximum for the same rupture location. In contrast, Δy is not affected to the same extent by θ, being maximum for s = 13 m. Note that this is opposite to what was observed for the pile group, where Δx was the one unaffected by θ. This is attributable to the different load transmission mechanisms of the two systems. While in the case of piled foundations the rotation of the pilecap is imposed through the piles, θ atop the caisson is solely due to the imposed differential displacement at its base. In stark contrast to the flexible pile group, the rigid caisson converts all of its base rotation to horizontal displacement at the top (i.e. at the pier base).

Finally, soil resilience is detrimental for the displacements (Δx and Δy) and the rotation (θ) at the pier base. The same conclusion is also valid for piled foundations, although our emphasis was on pile distress, for which exactly the opposite was shown (i.e. soil resilience to be beneficial).

6 Superstructure

Using the output of the first analysis step (Δx, Δy, and θ at the base of the pier), in Step 2 (*global* level) the response of the detailed model of the superstructure is analyzed. The discussions are restricted to typical results to develop qualitative insights on the response of selected bridge typologies. The focus is on typical viaducts, which are of greater importance compared to

the typical overpass bridge.

6.1 7-span viaduct

From the three investigated alternatives (see Fig. 4), two extreme cases are compared: (a1) continuous deck monolithically connected to piers; and (a3) 7 simply supported spans on elastomeric (seismic isolation) bearings.

The comparison is portrayed in Fig. 16 (referring to h = 2 m normal faulting at x = 150 m, i.e. under pier P3), in terms of deck vertical displacements Δy and bending moments M along the deck and the piers. In the first case (continuous deck monolithically connected to piers), the imposed tectonic deformation generates large stressing on both the deck *and the* piers (Fig. 16(a)). The tectonically-induced deck bending moments (black line) are an order of magnitude larger than their static (h = 0) values (in grey). Such stressing could not possibly be undertaken by any reasonable pre-stressed concrete box section — leading to failure. The stressing of the piers is also unacceptably intense.

The performance of the second alternative (7 simply supported spans on elastomeric bearings) is definitely favorable (Fig. 16(b)). In stark contrast to the statically indeterminate alternative, the imposed tectonic deformation does not cause any stressing of either the deck or the piers. The simply supported decks are only subject to rigid block type rotation and differential displacements. With adequate seating (to avoid deck falling), this alternative would survive even such a large tectonic deformation. Admittedly, the results shown herein refer to an extreme dislocation — deliberately to vividly illuminate the differences in response.

6.2 5-span viaduct

The response of the 5-span alternatives are compared next: (b1) continuous deck monolithically connected to piers; and (b2) continuous deck on elastomeric (seismic isolation) bearings. Note that due to the large 87.5 m span, a statically determinate solution cannot be considered realistic as such bridges are usually of the cantilevered-construction type.

The comparison is summarized in Fig. 17 (referring to only h = 0.5 m normal faulting at x = 131 m, i.e. at pier P2) in terms of deck Δy, and M along the deck and the piers. Although the imposed deformation is smaller (compared to h = 2 m that was imposed to the more flexible 7-span viaduct), it generates large distress in the first case (Fig. 17(a)). Due to the unavoidable increase of the deck cross-sectional stiffness (necessary to undertake the loads of the larger span), the deck bending moments are now even higher compared to the "lighter" 7-span viaduct. Evidently, such stressing would again lead to a failure of the deck *and* the piers.

The performance of the seismically isolated alternative is favorable (Fig. 17(b)). Although the system remains statically *indeterminate*, due to the insertion of "resilient" seismic isolation bearings between the piers and the deck, the tectonically-generated stressing is considerably reduced. The maximum M of the deck reduces from 450 MNm to 280 MNm, while the piers are almost insensitive to the imposed deformation. Naturally, even in this case the faulting-induced M is about 2.5 times larger than the maximum static (h = 0) bending moment. The results indicate that the seismically isolated alternative could marginally be designed to sustain this magnitude of bedrock offset. Design of the 5-span cantilever-construction bridge against larger offsets does not seem feasible.

7 Applications in Greece

The methodology developed herein has already been applied in real life for the design against tectonic deformation of: (i) a 70 m 3–span road bridge in the island of Rhodes, (ii) a 40 m 3–span road bridge in Southern Greece, and (iii) a major 400 m 3–span arched rail bridge in Central Greece. The last is presented in this section to illustrate the applicability of the methodology.

The 400 m viaduct bridge crosses an active fault zone that is associated with the 1954 Sofades $M \approx 7$ earthquake (Papastamatiou and Mouyaris, 1986). The length of the main rupture has been estimated to be on the order of 50 km with an average displacement of 1.8 m (Ambraseys and Jackson, 1990). With an estimated slip rate of 4 mm/year (Papadimitriou and Karakostas, 2003), the Sofades normal fault is the dominant seismotectonic feature of the broader area. Since the bridge is not directly crossing the main fault, but a secondary one, the seismotectonic study concluded that the bridge should be designed for a bedrock offset h = 30 cm.

The initial bridge design was a typical viaduct with 10 simply supported pre-stressed concrete spans with reinforced concrete piers, and founded through 3 x 3 pile groups (quite similar to the idealized alternative "a3" of this research). With the geotechnical profile mainly consisting of igneous periodite rock, initial FE analysis of the piled foundations showed that they could not possibly sustain the 30 cm design tectonic displacement. To satisfy the stringent design requirement that the bridge remains operational after the design seismic event (in order to avoid derailment, and to keep the rail network under operation), the largest post-earthquake longitudinal inclination should not exceed 20 %. The only way to achieve this was to increase the span length, by reducing the number of spans from 10 to 3.

As illustrated in Fig. 18, the improved design consists of three steel arch-type spans lying on seismic isolation spherical sliding bearings. The latter were selected as the best compromise in terms of bridge performance to tectonic deformation and strong seismic shaking. They provide adequate restoring force *and* large permanent deformation limits. Shock transmission units are also installed between the piers and the decks to

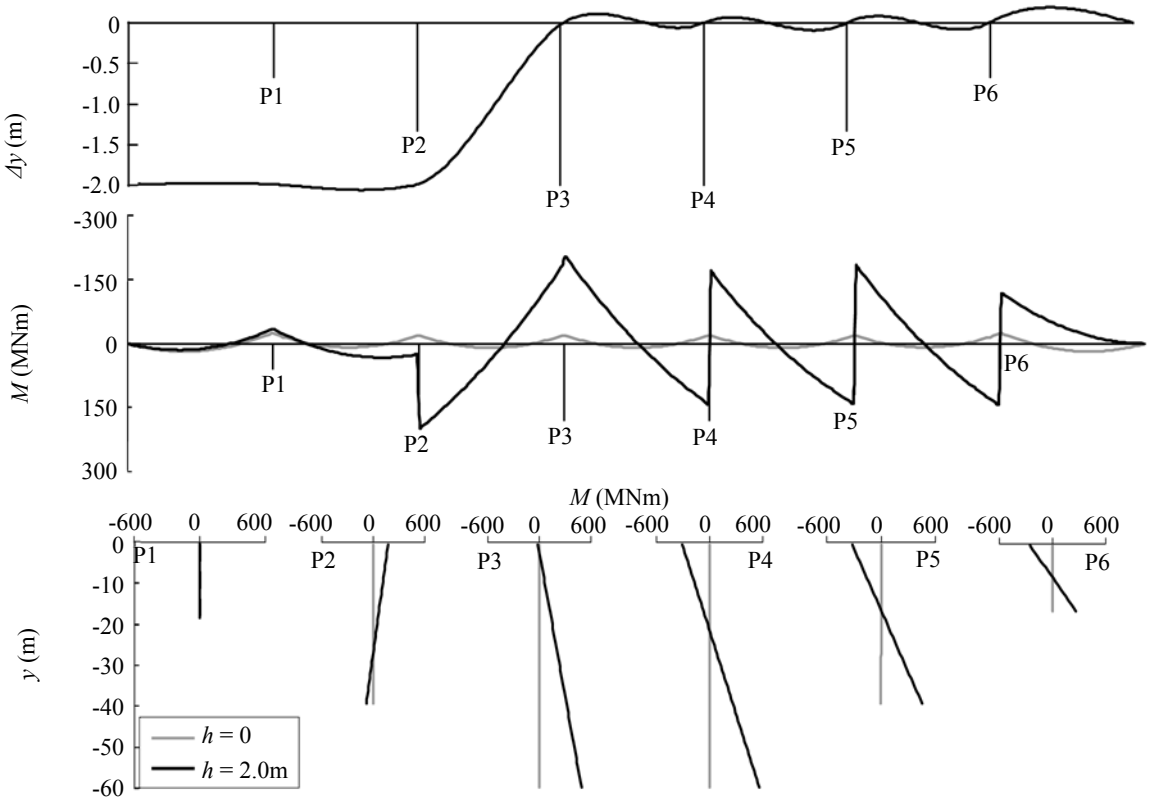

(a) Continuous deck monolithically connected to piers

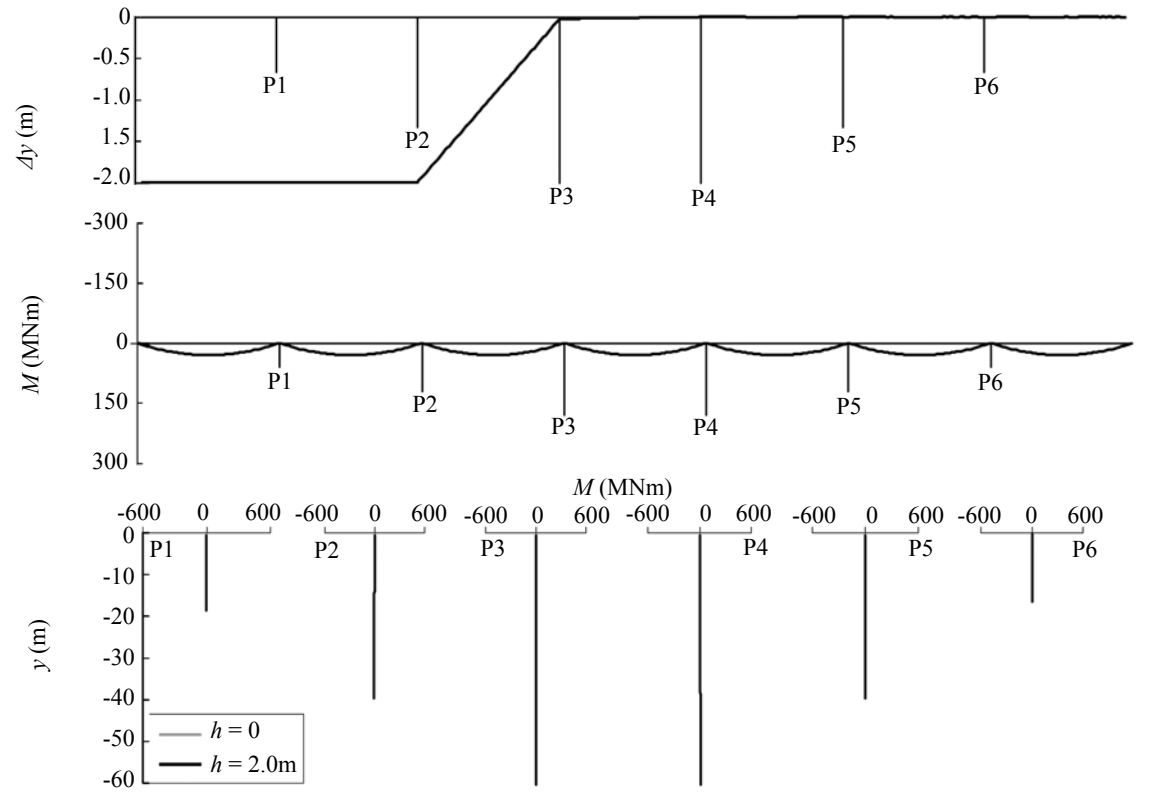

(b) 7 simply supported spans on elastomeric bearings

Fig. 16 7-span viaduct subjected to h = 2 m normal faulting at x = 150 m (i.e. at pier P3). Deck vertical displacement Δy and bending moments M of deck and piers

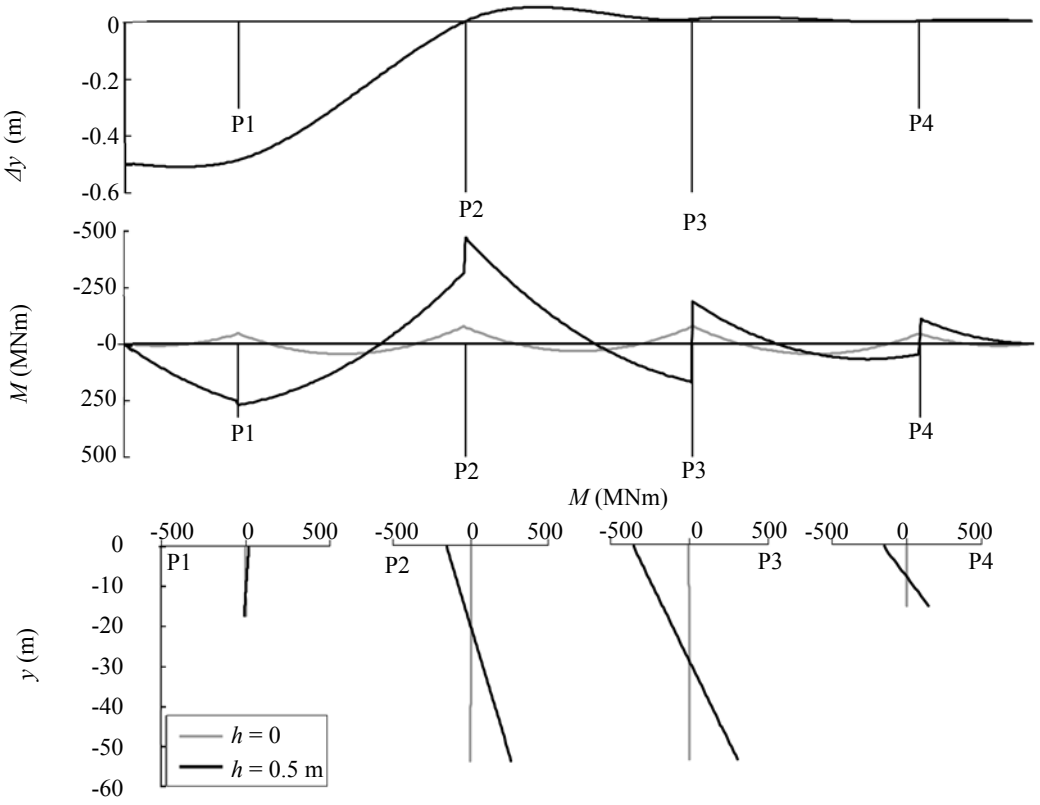

(a) Continuous deck monolithically connected to piers

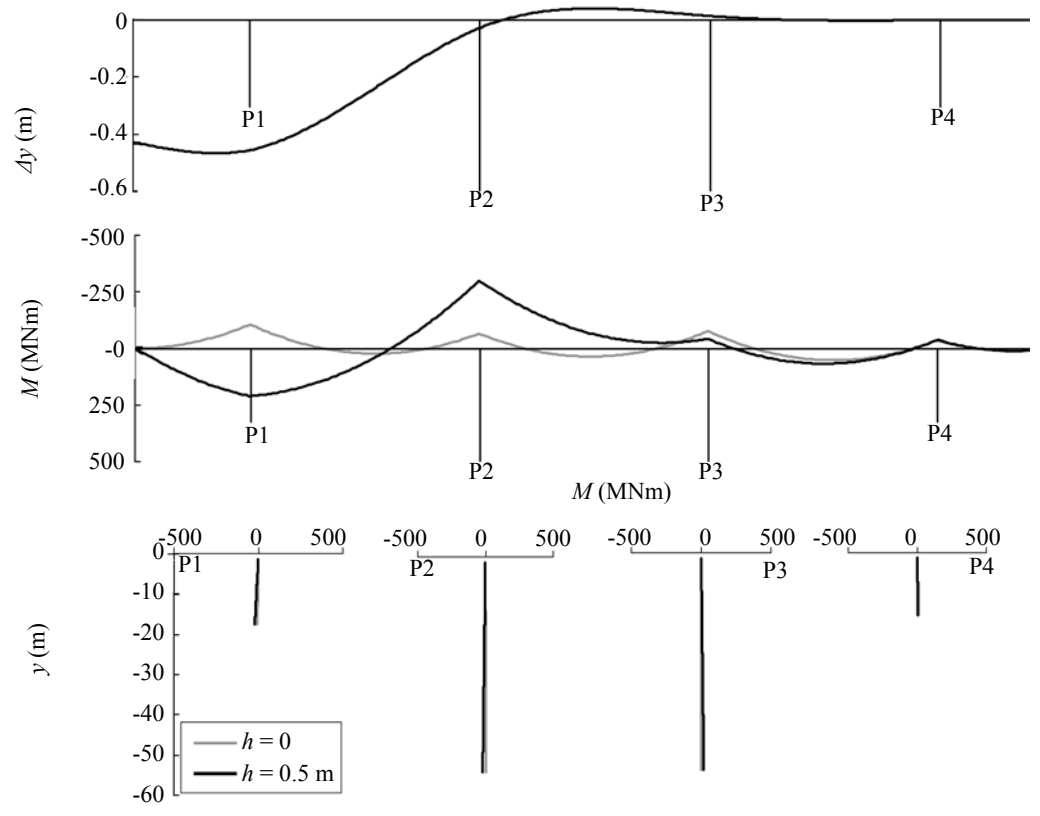

(b) Continuous deck on elastomeric seismic isolation bearings

Fig. 17 5-span viaduct subjected to h = 0.5 m normal faulting at x = 131 m (i.e. at P2). Deck vertical displacement Δy and bending moments M of deck and piers

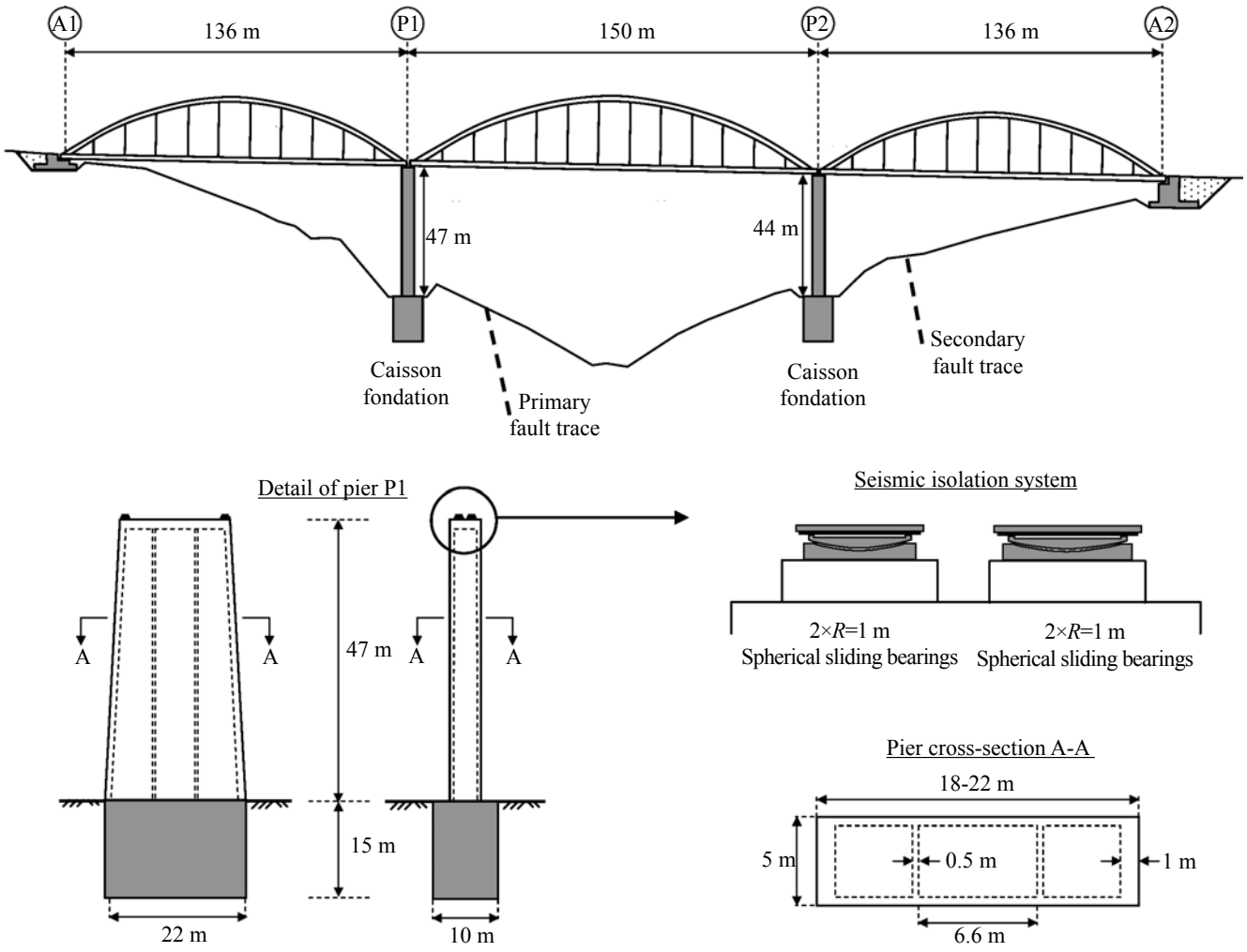

Fig. 18 Example application in Greece : the 3-span Domokos rail bridge, designed for h = 30 cm of normal bedrock offset. The initial bridge design (10 simply supported spans founded through 3 x 3 pile groups) was modified to cope with the design tectonic deformations

act as additional dampers in case of a strong earthquake. Such devices are activated only with large velocity, and do not react to pseudo-static loading such as the tectonic deformation. Given the results of this research, rigid 10m × 22m × 15m caissons were selected for the foundation of the two hollow reinforced concrete (44 m and 47 m tall) piers.

With the methodology presented herein, the bridge was analyzed for the design fault offset. Following the concept of Fig. 3, the response of a single bridge pier (*Step 1*) was analyzed first. Since the decks are seismically isolated, the lateral spring K_x was estimated on the basis of an equivalent tangent stiffness of the spherical sliding bearings; K_θ was assumed to be zero. Although the fault trace is clearly mapped, bearing in mind that the exact location of a fault rupture cannot be predicted accurately (e.g. Faccioli *et al*., 2008), the location of the fault rupture was parametrically investigated, both at the *local* (pier) and at the *global* (bridge) level.

At the *local* (pier-foundation) level, four scenarios were investigated with respect to the location of fault rupture location: s = 5, 9, 13, and 16 m. The results are summarized in Fig. 19. Note that the maximum rotation appears at the base of the pier for s = 13 m, while the maximum vertical and horizontal displacements are observed for s = 16 m. Since the relative effect of Δx, Δy, and θ on the various components of the bridge superstructure (decks, piers, seismic isolation bearings, joints, etc) cannot be predicted with certainty, two *local* fault rupture scenarios are used in the *global* analysis of the bridge:

(i) Scenario "a" (fault rupture at s = 13 m): Δx = 18.7 cm, Δy = 26.3 cm, and θ = 0.11º;

(ii) Scenario "b" (fault rupture at s = 16 m): Δx = 17.7 cm, Δy = 17.1 cm, and θ = 0.24º.

Based on the results of the *local* level FR–SFSI analysis, seven different tectonic loading combinations,

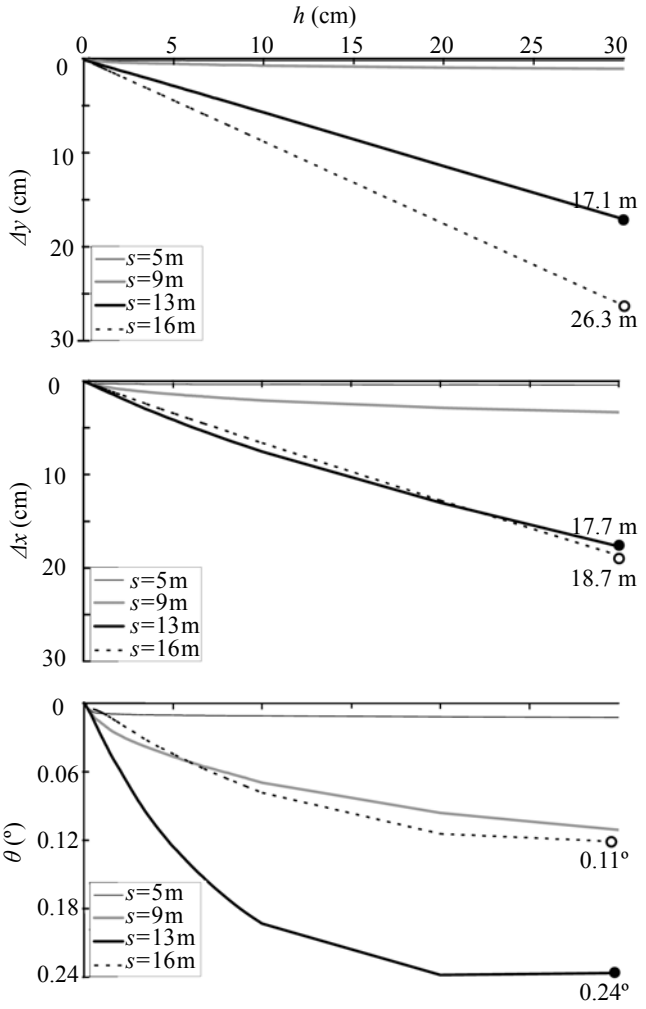

Fig. 19 Synopsis of analysis results for the 10 m × 22 m × 15 m caisson: Evolution with bedrock offset h of vertical Δy and horizontal Δx displacement, and rotation $\Delta\theta$ at the base of the pier for the four locations s of fault outcropping

as illustrated schematically in Fig. 20, are considered for the *global* level analysis of the superstructure. These combinations were then used to analyze the response of the bridge superstructure (*Step 2*). The seismic isolation devises, the seating of the decks, and the capacity of the joints were designed on the basis of the results of this analysis.

8 Conclusions and limitations

This paper has presented a general methodology for the design of bridges against large tectonic deformation. The problem is decoupled in two analysis steps: the first (*local* level) with the response of a single bridge pier subjected to fault rupture deformation; and the second (*global* level) with the detailed model of the superstructure. At the *local* level, emphasis is given to *fault rupture soil-foundation-structure interaction* (FR-SFSI), with the superstructure modeled in a simplified manner to capture its kinematic constraints. The *output* of this *local* level analysis is treated as the *input* for the *global* analysis.

The main conclusions are as follows:

(1) The design of bridges against tectonic deformation is quite feasible with proper design. The method of analysis presented herein may form the basis for future Code provisions and requirements on the subject.

(2) In all cases investigated herein, the rupture path is strongly affected by the presence of the foundation. The emerging fault rupture is not only diverted, but is also subject to bifurcation and diffusion.

(3) Piled foundations are in general quite vulnerable to faulting-induced deformation. End bearing piles cannot sustain even moderate bedrock offsets. Floating piles show better performance, which is dependent on soil resilience. The latter is in general beneficial in terms of pile stressing, but not necessarily for the inflicted displacements and rotation at the base of the pier. A hinged pile–to–cap connection may provide substantial stress relief, allowing a floating piled foundation to sustain larger imposed fault offsets, even on the order of a meter.

(4) Rigid massive caisson foundations are clearly advantageous. The faulting-induced deformation will force the caisson to move and rotate as a rigid body, resulting in vertical and horizontal displacement and rotation at the pier base.

(5) The location of fault outcropping plays a major role. For both piled and caisson foundations, displacements and rotation at the pier base are not maximum for the same location of fault outcrop. Since the exact fault location would never be known precisely a-priori, its location relative to the foundation has to be parametrically investigated in design.

(6) Continuous, statically indeterminate, superstructure systems are in general disadvantageous (the deck is forced to follow the imposed differential displacements). Statically determinate systems (such as multiple separate simply supported decks), allowing relative displacement and rotation without stressing, are quite favourable.

(7) In the case of large span cantilever-construction bridges, where a statically determinate system is hardly possible, use of resilient seismic isolation bearings is advantageous. Due to their resilience, they absorb some of the stressing, allowing the superstructure to deform more “smoothly” and thus to be relieved.

(8) In all cases, special care should be taken to avoid falling of the deck due to excessive relative displacements. Ample seating and adequate restraining devices, such as stoppers, are a necessity.

It should be noted that although the *local* level analysis employed herein has been extensively validated through successful genuine predictions of

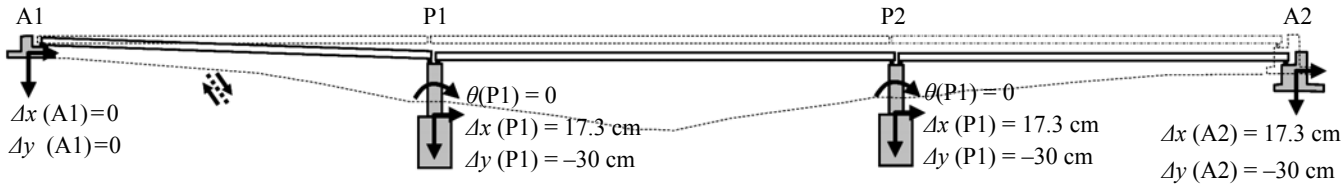

(a) Fault rupture between abutment A1 and pier P1

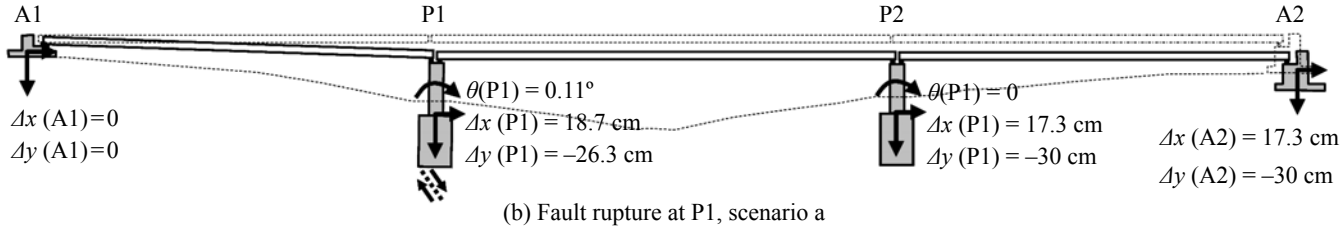

(b) Fault rupture at P1, scenario a

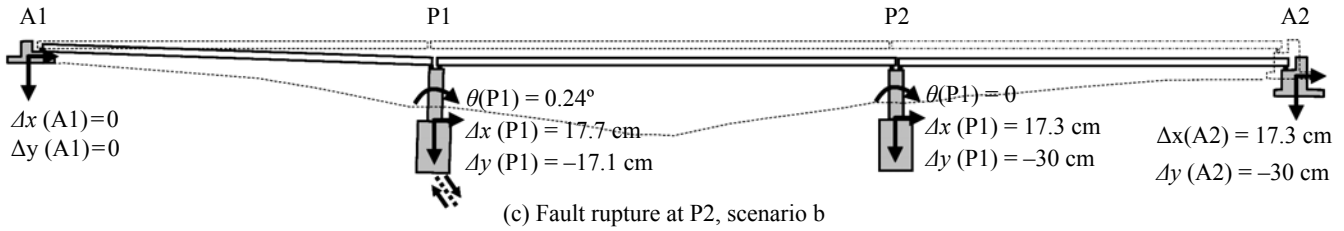

(c) Fault rupture at P2, scenario b

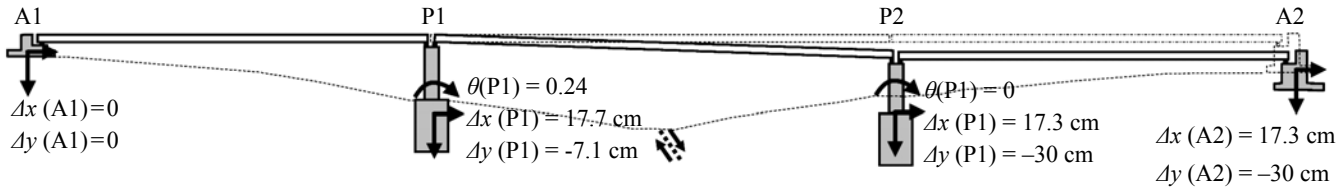

(d) Fault rupture between P1 and P2

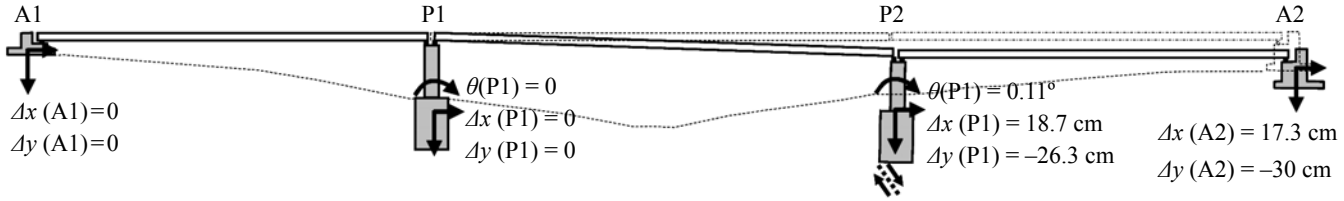

(e) Fault rupture at P2, scenario “a”

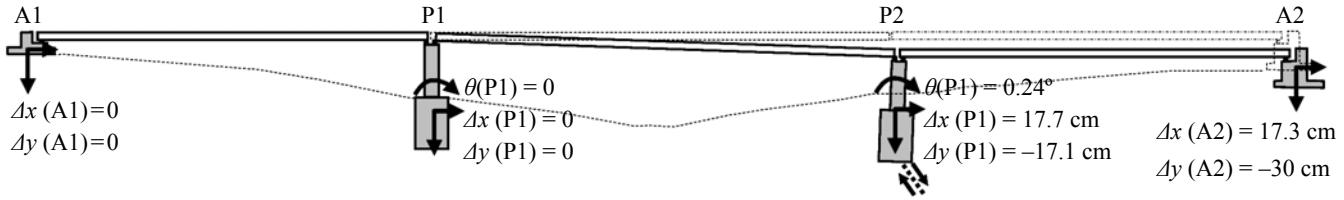

(f) Fault rupture at P2, scenario “b”

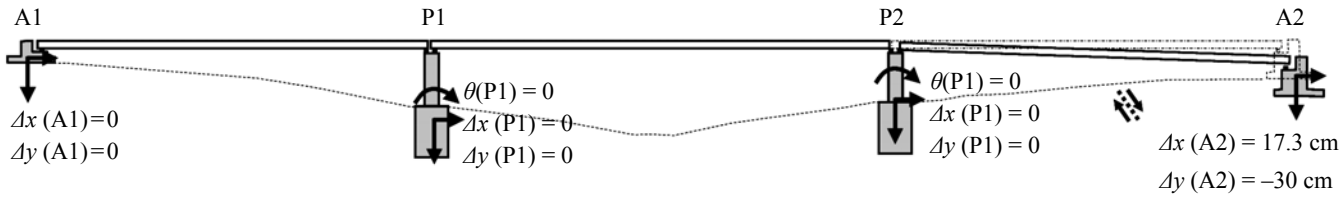

(g) Fault rupture between P2 and A2

Fig. 20 The seven tectonic loading combinations

centrifuge model tests, there are certain limitations: (a) all foundations (piled and caissons) are assumed to be in perfect contact with the bearing soil. This means that the developing forces upon the piles due to the outward and downward moving "hanging wall" may be somewhat exaggerated. Soil sliding around the piles or the caisson would tend to reduce the magnitude of such "drag" forces, leading to smaller pile distress and pile cap rotation and displacement; (b) scale effects are taken into account only in an approximate manner; and (c) the effect of excess pore water pressures has not been investigated. If the foundation is located under the water table, the response may be altered due to different effective stress conditions.

Acknowledgements

This work was funded by OSE (the Greek Railway Organization), as part of the research project "Railway Bridges on Active Seismic Faults." The authors gratefully acknowledge the structural engineers of Domokos Bridge, especially Mr. Ioannis Malios and his associates, for their cooperation and thoughtful comments.

References

Ambraseys NN and Jackson JA (1990), "Seismicity and Associated Strain of Central Greece Between 1890 and 1988," *International Journal of Geophysics*, **126**(3): 663–708.

Anastasopoulos I and Gazetas G (2007a), "Foundation-structure Systems over a Rupturing Normal Fault: Part I. Observations After the Kocaeli 1999 Earthquake," *Bulletin of Earthquake Engineering*, **5**(3): 253–275.

Anastasopoulos I and Gazetas G. (2007b), Behaviour of Structure–foundation Systems over a Rupturing Normal Fault: Part II. Analysis of the Kocaeli Case Histories," *Bulletin of Earthquake Engineering,* **5**(3): 277–301.

Anastasopoulos I, Gazetas G, Bransby MF, Davies MCR and El Nahas A (2007), "Fault Rupture Propagation Through Sand: Finite Element Analysis and Validation Through Centrifuge Experiments," *Journal of Geotechnical and Geoenvironmental Engineering*, ASCE, **133**(8): 943–958.

Anastasopoulos I, Gazetas G, Bransby MF, Davies MCR and El Nahas A (2008), "Normal Fault Rupture Interaction with Strip Foundations," *Journal of Geotechnical and Geoenvironmental Engineering*, ASCE. (in print)

Anastasopoulos I, Gerolymos N and Gazetas G (2001), "Possible Collapse Reasons of an Access Span of the Nishinomiya-ko Bridge: Kobe 1995," *Proceedings of the 4th Hellenic Conference on Geotechnical Engineering*, Athens, Vol. 2, pp. 83–90.

Berill, JB (1983), "Two-dimensional Analysis of the Effect of Fault Rupture on Buildings with Shallow Foundations," *Soil Dynamics and Earthquake Engineering,* **2**(3): 156–160.

Bransby, MF, Davies MCR and El Nahas A (2008a), "Centrifuge Modelling of Normal Fault-foundation Interaction," *Bulletin of Earthquake Engineering, Special Issue: Integrated Approach to Fault Rupture- and Soil-foundation Interaction*. (in press)

Bray JD (1990), "The Effects of Tectonic Movements on Stresses and Deformations in Earth Embankments," *Ph.D. Dissertation*, University of California, Berkeley.

Bray JD (2001), "Developing Mitigation Measures for the Hazards Associated with Earthquake Surface Fault Rupture," *Workshop on Seismic Fault-induced Failures – Possible Remedies for Damage to Urban Facilities*, University of Tokyo Press, pp. 55–79.

Bray JD, Seed RB, Cluff LS and Seed HB (1994a), "Earthquake Fault Rupture Propagation Through Soil," *Journal of Geotechnical Engineering*, ASCE, **120**(3): 543–561.

Bray JD, Seed RB and Seed HB (1994b), "Analysis of Earthquake Fault Rupture Propagation Through Cohesive Soil," *Journal of Geotechnical Engineering*, ASCE, **120**(3): 562–580.

Brune JN and Allen CR (1967), "A Low-stress-drop, Low Magnitude Earthquake with Surface Faulting, The Imperial, California, Earthquake of March 4, 1966," *Bulletin of the Seismological Society of America*, **57**: 501–514.

Cole DA Jr and Lade PV (1984), "Influence Zones in Alluvium Over Dip-slip Faults," *Journal of Geotechnical Engineering*, ASCE, **110**(5): 599–615.

Duncan JM and Lefebvre G (1973), "Earth Pressure on Structures Due to Fault Movement," *Journal of Soil Mechanics and Foundation Engineering,* ASCE, **99**: 1153–1163.

Erdik M (2001), "Report on 1999 Kocaeli and Düzce (Turkey) Earthquakes," Casciati G, *Structural Control for Civil and Infrastructure Engineering*, Magonette: World Scientific.

Faccioli E, Anastasopoulos I, Callerio A and Gazetas G (2008), "Case Histories of Fault–foundation Interaction," *Bulletin of Earthquake Engineering, Special Issue: Integrated approach to fault rupture- and soil-foundation interaction*. (in press)

Gerolymos N and Gazetas G (2006a), "Winkler Model for Lateral Response of Rigid Caisson Foundations in Linear Soil," *Soil Dynamics and Earthquake Engineering*, **26**(5): 347–361.

Gerolymos N and Gazetas G (2006b), "Development of Winkler Model for Static and Dynamic Response of Caisson Foundations with Soil and Interface Nonlinearities," *Soil Dynamics and Earthquake Engineering*, **26**(5): 363–376.

Gerolymos N, Giannakou A, Anastasopoulos I and Gazetas G (2008), "Evidence of Beneficial Role of Inclined Piles: Observations and Numerical Results," *Bulletin of Earthquake Engineering, Special Issue: Integrated approach to fault rupture- and soil-foundation interaction*. (in press)

Hanlong L, Susamu I and Ichii K (1997), "Evaluation of Deformation to the Pneumatic Caisson Foundations of the Kobe Ohashi Bridge," *Report*, The Port and Harbor Research Institute, Japan.

Horsfield WT (1977), "An Experimental Approach to Basement-controlled Faulting," *Geologie En Mijnboyw*, **56**(4): 363–370.

Hwang HY (2000), *Taiwan Chi-Chi Earthquake 9.21.99. Bird's Eye View of Cher-lung-pu Fault*," Taipei: Flying Tiger Cultural Pub., pp. 150.

Jewell RA and Roth CP (1987), "Direct Shear Tests on Reinforced Sand," *Gétechnique*, **37**(1): 53–68.

Kawashima K (2001), "Damage of Bridges Resulting from Fault Rupture in The 1999 Kocaeli and Duzce, Turkey Earthquakes and The 1999 Chi-Chi, Taiwan Earthquake," *Workshop on Seismic Fault-Induced Failures–Possible Remedies for Damage to Urban Facilities,* University of Tokyo Press, pp. 171–190.

Niccum MR, Cluff LS, Chamoro F and Wylie L (1976), "Banco Central de Nicaragua: A Case History of a High-rise Building That Survived Surface Fault Rupture," Humphrey CB, *Engineering Geology and Soils Engineering Symposium, No. 14*, Idaho Transportation Department, Division of Highways, pp. 133–144.

Pamuk A, Kalkanb E and Linga HI (2005), "Structural and Geotechnical Impacts of Surface Rupture on Highway Structures During Recent Earthquakes in Turkey," *Soil Dynamics and Earthquake Engineering*, **25**: 581–589.

Papadimitriou EE and Karakostas VG (2003), "Episodic Occurrence of Strong (Mw ≥ 6.2) Earthquakes in Thessalia Area (central Greece)," *Earth and Planetary Science Letters*, **215**: 395–409.

Papastamatiou D and Mouyaris N (1986), "The Earthquake of April 30, 1954, in Sophades (Central Greece)," *Geophys. J.R. Astron. Soc.*, **87**: 885–895.

Slemmons DB (1957), "Geological Effects of the Dixie Valley-fairview Peak, Nevada, Earthquakes of December 16, 1954," *Bul. of the Seism. Soc. of America*, **47**(4): 353–375.

Taylor CL, Cline KM, Page WD and Schwartz DP (1985), "The Borah Peak, Idaho earthquake of October 28, 1983 – Surface Faulting and Other Phenomena," *Earthquake Spectra*, **2**(1): 23–49.

Tazoh T, Ohtsuki A, Aoki T, Mano H, Isoda K, Iwamoto T, Arakawa T, Ishihara T and Ookawa M (2002), "A New Pile-head Device for Decreasing Construction Costs and Increasing the Seismic Performance of Pile Foundations, and Its Application to Structures," *Proc. 12th European Conference on Earthquake Engineering*, Paper No. 720, Elsevier Science Ltd..

Ulusay R, Aydan O and Hamada M (2002), "The Behaviour of Structures Built on Active Fault Zones: Examples from the Recent Earthquakes of Turkey," *Structural Engineering & Earthquake Engineering*, JSCE, **19**(2): 149–167.

Youd TL (1989), "Ground Failure Damage to Buildings During Earthquakes," *Foundation Engineering Current Principles and Practices*, Vol. 1, pp. 758–770. New York: ASCE.

Youd TL, Bardet JP and Bray JD (2000), "Kocaeli, Turkey, Earthquake of August 17, 1999 Reconnaissance Report," *Earthquake Spectra*, **16** (Suppl. A): 456.